R. & M. No. 3287

MINISTRY OF AVIATION

AERONAUTICAL RESEARCH COUNCIL
REPORTS AND MEMORANDA

A Comparison of Results in the A.R.A. Transonic Tunnel on a Small and a Large Model of a Slender Wing

By T. E. B. Bateman, B.A. and A. B. Haines, B.Sc.

LONDON: HER MAJESTY'S STATIONERY OFFICE
1962
PRICE 14*s.* 6*d.* NET

A Comparison of Results in the A.R.A. Transonic Tunnel on a Small and a Large Model of a Slender Wing

By T. E. B. BATEMAN, B.A. and A. B. HAINES, B.Sc.

*Reports and Memoranda No. 3287**
September, 1961

Summary. Force, moment and pressure-plotting measurements are reported on 75 deg slender wings of 60 in. and 20 in. lengths in the Aircraft Research Association 9 ft × 8 ft perforated-wall transonic tunnel. The object of the tests was to obtain some idea of the tunnel-interference corrections for slender-wing models.

The maximum blockage correction on lift-curve slope for the larger model which has a blockage ratio of 0·36 per cent reduces an apparent Mach number of 1·00 to 0·975. Earlier tests on a swept-wing model with a blockage ratio of 0·5 per cent gave a correction of only about 0·02 in M, and hence the new results confirm the expectation that transonic interference for a given blockage ratio may be larger for slender models. No blockage correction on aerodynamic-centre position appears to be needed and it is explained that this could be due to the effect of the variation of blockage along the length of the model.

Reflected wave-type interferences on the larger model has the effect of changing the steep rise in C_D between $M = 0{\cdot}99$ and $M = 1{\cdot}01$ into a relatively slow rise to a maximum near $M = 1{\cdot}10$ at which C_D is about 0·001 too high. This is due mainly to reflections of the bow shock and forward compression region. The walls would have been more effective in alleviating these reflections if the models had been placed further forward in the working section. Also, it is probably true that the bow shock was somewhat stronger with these models than with other more typical slender wings.

The results suggest that in general, tests on slender-wing models placed at the most suitable position in the tunnel should give reasonably interference-free results at Mach numbers above about $M = 1{\cdot}1$. On the basis of the evidence presented in this paper, it should be possible to devise corrections even in the range $M = 1{\cdot}0$ to $1{\cdot}1$ particularly if a few pressure-plotting points are included in the models under test.

1. *Introduction.*

Many slender delta- and ogee-wing models are now being tested in the A.R.A. 9 ft × 8 ft perforated-wall transonic tunnel. Such wings would normally be designed to cruise at some Mach number beyond $M = 1{\cdot}4$ and hence outside the range of the tunnel but it is still important to obtain data appropriate to the climb and off-design cruise conditions of flight. More specifically, tests at transonic speeds are required to find the maximum values of C_{D0} and possibly $(\partial C_L/\partial\alpha)_M$, to determine the magnitude and nature of the transonic shift in the aerodynamic-centre position and whether this occurs smoothly or is preceded by a forward shift, and to check that no strong shock waves are present on the wing ahead of the trailing edge at any Mach number. For wings with little trailing-edge sweep, all these characteristics are most likely to occur in a small

* Previously issued as A.R.A. Wind Tunnel Note No. 42—A.R.C. 23,237.

range of Mach number on either side of $M = 1{\cdot}0$, *i.e.*, just in the range where tunnel-interference effects are at their largest and least predictable. Some quantitative idea of these interference effects is therefore vital if reliable conclusions are to be drawn from the tests. This is more important than in the case of a highly swept wing for which critical conditions may be delayed to beyond this Mach number range and for which, as a result, it may be easier to fair the data through $M = 1{\cdot}0$.

Considerable insight into the general nature and possible magnitude of both blockage and wave-reflection types of interference in the A.R.A. tunnel was gained from a programme of tests on various models of a swept-wing-body configuration. These models had the same geometry but differed in scale; the results and conclusions have been reported in detail in Ref. 1. Strictly, however, this evidence should only be applied quantitatively to models of a broadly similar type and it seemed desirable to repeat the exercise for two slender-wing models. Quite apart from the importance of being able to apply accurate corrections to the results on slender wings, there were various reasons for believing that the interference could become more serious for slender shapes. First, theoretical studies by both Berndt[2] and Page[3], supported by experimental results on simple bodies of revolution[3, 4] had shown that tunnel interference near $M = 1{\cdot}0$ could be greater for models of high fineness ratio. This should certainly be true for models of a given blockage ratio and even possibly for models of a given length. Secondly, the wave-reflection effects could be quite different for the slender wings in view of the different character of the incident-flow field. This will be explained more fully later in the report but one illustration can be quoted here. The reflection of the bow shock from the tunnel walls at low supersonic Mach numbers would probably reflect back somewhere on the surface of a slender-wing model whereas with the swept-wing-body combination of Ref. 1, it would reflect ahead of the wing leading edge.

It was decided therefore to test two slender-wing models having roughly the same geometry but being 20 in. and 60 in. long respectively. Unfortunately the choice of model was dictated by what was available at the time and in several respects, the geometry of these models is somewhat unrepresentative of the slender-wing designs now being tested. For example, the models, which were designed and manufactured at a comparatively early stage in the present phase of slender-wing research, are delta wings with rounded leading edges, and also, relatively large body fairings to house the sting and balance are present. Viewed in the present context, these features are troublesome, first in that some of the differences between the results for the large and small models are probably due to the different test Reynolds numbers rather than to tunnel interference and secondly, almost certainly, the bow shock at low supersonic Mach numbers is stronger than with most of the slender-wing designs now being tested and hence, reflections of this bow shock and forward compression region are correspondingly greater.

Both overall force and moment and pressure-plotting measurements were made. The balance results give some idea of the overall significance of the blockage or wave-reflection interference while the pressure-plotting results enable the details of the interference to be better understood and be applied to other models.

2. *Details of Models and Tunnel.* 2.1. *Model Geometry.* Both the large and small models were manufactured by the Royal Aircraft Establishment, for tests in their 8 ft and 3 ft tunnels respectively, and were loaned to A.R.A. for these tests. The main geometry and dimensions of the models are shown in Fig. 1a. Apart from minor differences they are scale versions of the same geometry.

They are symmetrical deltas with 75 deg leading-edge sweep and aspect ratio 1·072. The wing section is 4½ per cent thick, RAE 101 having its maximum thickness at 0·31c and a round leading edge. The centreline chords of the two models are 60 in. and 20 in. respectively. The blockage ratios based on maximum cross-sectional area in the 9 ft × 8 ft tunnel are 0·36 per cent and 0·04 per cent. The ratio of sting-fairing diameter to maximum wing thickness is 1·65, and of wing area to base area is 64 for the large model and 61 for the small model. Pressure-plotting-hole positions are shown in Figs. 1b and c, and it is seen that the small model has four spanwise rows of holes and the large model has four chordwise rows.

The minor differences referred to can be seen in Fig. 1a. The large model has a slightly bluffer nose to its fairing, and the fairing extends 5 per cent of c_0 behind the trailing edge. The small model has its tips cropped an insignificant amount. The only one of these differences likely to be at all noticeable is the bluffness of the fairing. Another point is that the so-called sting fairings extend almost to the wing apex and would perhaps be better termed fuselages than fairings.

2.2. *Relative Geometry of Models and Tunnel.* Details of the tunnel working section are given in Ref. 1 and the longitudinal positions of the models in the tunnel are shown in Fig. 1d. This also shows some of the properties of the four perforated tunnel walls.

The centre of rotation of each model, $\frac{2}{3}c_0$, is at the same position in the tunnel. The tunnel working section is 8 ft × 9 ft and, since the models are placed 6 in. above the tunnel centreline, their distance from the roof is 42 in. and from the floor and side walls is 54 in.

The perforations of the tunnel walls commence 40 in. upstream of the nose of the large model and the open-area ratio then increases to a maximum of 22½ per cent at 28 in. downstream of the nose, and maintains this value until the perforations end 106 in. downstream of the nose. The tunnel floor near the model is a moveable section and the front of it is of saw-tooth shape near the start of the porosity. The saw teeth can give rise to small disturbances in the flow.

Other details of Fig. 1d are discussed later.

3. *Tests and Measurements.* Overall lift, drag and pitching moment were measured from $M = 0{\cdot}6$ to 1·4 and from $\alpha = -2$ deg to $+8$ deg in ½ deg steps with traverses from -8 deg at some Mach numbers. Following these incidence traverses, a run at zero incidence was made through the test Mach number range. These results were obtained from a six-component balance (R.A.E. 3 in. F) for the large model, and on a two-moment-station sting balance and separate axial-force unit for the small model.

Pressure-plotting tests were made over the Mach number range 0·94 to 1·4 at zero incidence, with traverses in 1 deg steps up to 8 deg at $M = 0{\cdot}98$ and 1·06 only. Pressures were measured on mercury manometers.

All the tests were originally made with ½ in. wide bands of grade 220 carborundum on both surfaces near the leading edge. The drag measurements on the large model in the first tests appeared to be too low, and it was suspected that transition had not been fixed. These tests were therefore repeated with a roughness band extended back 1 in. from the leading edge on both surfaces; the results then appeared much more plausible.

The tests were made at atmospheric stagnation pressure, and the Reynolds number, based on centreline chord, increased from 5·6 to 7·4 × 10^6 for the small model as the Mach number varied from 0·6 to 1·4, and from 16·8 to 22·2 × 10^6, for the large model.

Due to the very low blockage of the small model, the tunnel speed could not always be held at the usual Mach numbers for the tunnel-liner settings at $M = 1{\cdot}19$ and above. Thus the small model had to be tested sometimes at $0{\cdot}01$ in M above the usual Mach numbers in this range. This could mean that small buoyancy effects were introduced.

4. *Accuracy and Presentation of Results.* The Mach number was at times $0{\cdot}003$ below the nominal value and this has been taken into account in plotting the overall results against M. Pressure-plotting tests were made at nominal Mach numbers without further corrections. The variation of Mach number during an incidence traverse was at the most $\pm 0{\cdot}002$. Mach number was calculated from plenum pressure; its local variation along the tunnel centreline (Ref. 4) is less than $\pm 0{\cdot}005$ up to $M = 1{\cdot}1$ but increases to a maximum of $\pm 0{\cdot}016$ at $M = 1{\cdot}4$ and possibly slightly more than this for the small model which had to be tested at off-design Mach numbers for $M > 1{\cdot}19$.

The majority of the force results lie within a scatter band of $\pm 0{\cdot}001 C_L$, $\pm 0{\cdot}0002 C_m$ and $\pm 0{\cdot}0002 C_D$. This accuracy also applies to the variation of any force taken from a mean value on a curve and referred to a datum at $M = 0{\cdot}8$, *e.g.*, the variation of zero-lift drag with M in Fig. 6. The absolute values of the results are accurate to $\pm 0{\cdot}002$ in C_L, $\pm 0{\cdot}0005$ in C_m and $\pm 0{\cdot}0005$ in C_D.

Incidence was set to within $0{\cdot}03$ deg and corrected for deflections under load (in the force tests) which amounted to $0{\cdot}5$ deg at maximum load. However, at the time of these tests there was an upwash in the tunnel varying by $0{\cdot}25$ deg over the Mach number range. The lift curves have been corrected for this upwash and balance drift on the normal force channel, and it is seen from Fig. 2 that they pass through the origin. The symmetry of the C_D versus C_L curves, which is sensitive to the accuracy of both zero incidence and zero lift, is satisfactory in all cases except between $M = 1{\cdot}00$ and $1{\cdot}10$ (Fig. 4). The asymmetry here is of the order of $0{\cdot}05$ deg in incidence and $0{\cdot}002$ in C_L, in such a sense as not to change the final $C_L - \alpha$ curves, and neither will it affect the zero-lift drag.

Care was taken in the pressure-plotting tests to set the models at the same incidence, but unlike the force tests, this has not been corrected for tunnel upwash. The nominal incidence may therefore be $0{\cdot}25$ deg off the true value but the comparison between models should not be significantly affected. Over most of the wing surface, C_p would change by about $0{\cdot}004$ for this angle and this is also the width of the scatter band of the pressure measurements. Since the small model had four spanwise rows of pressure holes and the large model four chordwise rows, the measurements of the small model have been interpolated to give comparisons on the same chords as the large model. Also some additional evidence has been used from lower-surface holes (Fig. 1b) to cover more of the wing area near the centreline.

Results are presented graphically for C_L, C_m, C_D, and derived results have been obtained from large-scale plots not shown here. Pitching moment is referred to a position $\frac{2}{3} c_0$. Derived results are shown *versus* Mach number for lift-curve slope (taken over ± 1 deg incidence) and aerodynamic centre (over $\pm 0{\cdot}05 C_L$) together with C_{D0} and base pressure. Nominal Mach numbers are quoted on the basic curves, but the derived points are plotted against the true Mach numbers of the tests.

Only a selection of the pressure-plotting results is shown to illustrate the main effects. In particular the pressures at $0{\cdot}25$ and $0{\cdot}45$ semi-span are used, since those at $0{\cdot}65$ and $0{\cdot}85$ have only one common point between the models.

5. *Some General Notes on Tunnel Interference.* 5.1. *Constraint and Blockage.* These two types of interference are met with in subsonic tunnels. The term constraint may be applied to various

types of interference but it is here used with its usual meaning to refer to the distortion of the flow field by the tunnel walls which leads to effective changes of incidence, camber and induced drag. The corrections for constraint are of opposite sign depending on whether the tunnel has solid walls or is an open jet. Since the perforated walls of the transonic tunnel provide boundary conditions somewhere between the two types of tunnel just mentioned, it is reasonable to expect the constraint corrections to be nearer zero than for the other types of tunnel. Comparisons of subsonic tests on a swept-back wing in the A.R.A. tunnel with those of the same model in a solid-wall tunnel have provided evidence of a small constraint correction to incidence of the same sign as for an open-jet tunnel, *i.e.*, the measured lift-curve slope is too low. However, the correction in the A.R.A. tunnel should be small for the present models in view of their very low aspect ratio and therefore constraint will not be considered further in this report.

The second type of interference in a subsonic tunnel, blockage, also varies in sign depending on whether the tunnel has solid walls or an open jet. Once again, the perforated walls greatly reduce the interference but there is nevertheless still a significant correction required for blockage and it is of the same sign as for an open-jet tunnel. Thus the apparent Mach number tends to be too high in the transonic region. The need for a correction of this sort has been found previously by comparison of models of different blockage ratios (*e.g.*, Ref. 1) and of tunnel tests with free-flight results. Also theoretical estimates have been made (Refs. 2, 3).

5.2. *Terminal-Shock Movement.* It is now well established that the rearward movement of the terminal shock near $M = 1{\cdot}0$ is retarded by the tunnel walls, and this has been analysed for the standard swept-wing calibration models in transonic tunnels in Ref. 1. The physical explanation is briefly illustrated by reference to a body with a supersonic expansion field near the nose, which reflects from the sonic line as a shock further aft on the model. When this expansion field is cut by the tunnel walls instead of the sonic line, the terminal shock will be further forward.

5.3. *Wave-Reflection Interference.* Tunnel interference of this nature occurs in the Mach number range from near $M = 1{\cdot}0$ up to the stage when all reflected waves are sufficiently clear of the model base to lose their influence on the model. In the present tests, the strength of the waves, when they have crossed the base, is sufficiently weak for them to be neglected, so this interference need only be considered up to the Mach numbers when reflected waves actually cross the base itself.

In the present case, waves and their reflections are assumed to lie at the Mach angle corresponding to the tunnel free-stream Mach number, and the tunnel boundary layer is assumed to form a reflecting surface at 3 in. from the wall rather than at the wall itself. This approach was used satisfactorily in analysing the pressure-plotting results of Ref. 1. The reflections from the tunnel roof cross the model after those from the other walls, since it lies nearer the model. Assuming the bow shock originates from the model nose itself and has no curvature, its reflection finally crosses the base of the small model at about $M = 1{\cdot}03$ and the large model at $M = 1{\cdot}26$. The fact that the actual bow shock is curved and detached from the nose causes the reflected disturbance to clear the base at somewhat higher Mach numbers.

Fig. 1d shows two curves relating the tunnel Mach number with the position at which an idealised bow shock, attached to the nose of the large model, meets either the roof or the floor and side walls. It also shows the variation of Mach number along the tunnel for which the local open-area ratio cancels incident compression waves, as determined from the experiments in Ref. 1. An incident shock wave is reflected as a shock if the open-area ratio is too small and as an expansion if it is too

large, and a similar argument applies to incident expansion waves. Thus Fig. 1d indicates the ranges when the idealised bow shock of the large model is reflected as an expansion or a shock or is cancelled by the wall. For the shock which strikes the roof, it is seen that the wall is too open for Mach numbers below 1·14 so it will be reflected as an expansion, and above $M = 1{\cdot}14$, the wall is too closed and it will be reflected as a shock. However, for Mach numbers between about 1·10 and 1·19, the wall porosity is almost correct to cancel the incident wave and any reflections will be very weak. Similar arguments apply to all other wave reflections. Analysis has shown that also crossing the model is a reflected-wave disturbance from the saw-tooth junction on the floor.

5.4. *Other Interference Effects.* Perhaps the most important other factor is the possibility of a buoyancy effect which would require a correction to the measured drag data. The calibration of the empty tunnel showed that for a typical model such as the larger model tested here, these corrections should be negligible until beyond $M = 1{\cdot}2$. The precise value obviously depends on the wing thickness distributions and so should be calculated for any particular model. A typical value for a large slender-wing model would be a correction of 0·0002 in C_D at $M = 1{\cdot}4$. The presence or otherwise of a correction for a small model will also depend on where the model is located along the tunnel centreline *i.e.*, where the model is relative to the various perturbations in the Mach number distributions at the higher Mach number.

6. *Overall Results.* These are first discussed independently and then again later in connection with the pressure-plotting results.

6.1. *Lift.* The $C_L - \alpha$ curves and the variation of $(\partial C_L/\partial\alpha)_M$ with Mach number at zero incidence are shown in Figs. 2 and 5. Allowing for scatter, the values of $(\partial C_L/\partial\alpha)_M$ for the two models begin to diverge at about $M = 0{\cdot}93$. The most striking differences occur in the region of the rapid increase in lift-curve slope with Mach number near $M = 1{\cdot}0$. For the small model (0·04 per cent blockage) this rapid increase occurs between $M = 0{\cdot}98$ and 1·00, whereas for the large model (0·36 per cent blockage), it is between $M = 1{\cdot}00$ and 1·02. It should be noted when determining blockage corrections that blockage affects the results in two respects. In addition to increasing the apparent Mach number, the coefficients are based on too high a dynamic pressure and hence are too small. These two effects can be seen in Fig. 5, *e.g.*, at the start of the rapid increase in $(\partial C_L/\partial\alpha)_M$, the value of $(\partial C_L/\partial\alpha)_M$ is lower on the large model.

This difference in blockage of $\Delta M = 0{\cdot}02$ between the two models is rather greater than the value (0·015) which would be derived from theoretical predictions or from the pressure-plotting data (*see* 7.1). It should be noted however that pressure-plotting evidence is not available over the full chord.

The discussion above has been based on the values of lift-curve slope at zero incidence which are the same for the two models for Mach numbers below 0·9 and above 1·2. This is not true at higher incidences for Mach numbers below $M = 1{\cdot}1$. The large model then gives about 5 per cent less lift. The pressure-plotting results confirm that this is because the vortex development from near the rounded leading edge is somewhat delayed on the large model. Almost certainly, this is due to the different test Reynolds numbers. The influence of this vortex on the lift-curve slope will become less as the Mach number is increased and this should account for the improved agreement between the results for the two models at the higher Mach numbers.

6.2. *Pitching Moment.* $C_m - C_L$ curves are shown in Fig. 3 and the variation of aerodynamic-centre position with Mach number is plotted in Fig. 5. The scale used for C_m is very sensitive and in view of the basic non-linearity of the curves, the apparent scatter is not serious. The general tendency, even at low subsonic speeds, is for the aerodynamic centre for the large model to be about 1 per cent of $\bar{c}$ further aft. This is probably due mostly to the difference in test Reynolds number and perhaps partly to the small geometric differences between the models, *e.g.*, the extended sting fairing behind the trailing edge of the large model.

Apart from this basic difference in aerodynamic-centre position, there are no significant discrepancies between the pitching moment of the two models below $M = 0{\cdot}94$ or above $M = 1{\cdot}10$. Even near $M = 1{\cdot}0$, the pitching-moment results do not suggest the need for a blockage correction. On both models, the rapid transonic rearward shift of the aerodynamic centre occurs between $M = 0{\cdot}98$ and $M = 1{\cdot}02$. At $C_L = 0{\cdot}1$, there is a difference of about $0{\cdot}01$ in M for the rearward movement (Fig. 5).

At first sight, the absence of any apparent blockage effect on the aerodynamic-centre variation appears to conflict with the evidence from the lift and pressure-plotting data. It is worth noting that a similar contrast is observed for the results in Ref. 1 for the swept wing-body calibration models. A possible explanation of this apparent paradox is given later in the analysis of the pressure-plotting data.

At Mach numbers beyond $M = 1{\cdot}0$, there are some small fluctuations in aerodynamic-centre position which may be due to reflected-wave interference. Pitching moments for the two models are the same at $M = 1{\cdot}19$ and $1{\cdot}30$, while the small difference at $M = 1{\cdot}40$ at the higher incidences is thought to be connected with the slightly different Mach number distributions along the models at this extreme point. All these effects above $M = 1{\cdot}0$ are however relatively minor.

One final point about the pitching moments is that since the models are symmetrical, $C_{m\,0}$ should be zero and in fact, no value greater than $0{\cdot}0005$ was observed. An interference effect is theoretically possible because the models are not mounted on the tunnel centreline but the evidence appears reassuring. It is therefore probable that tunnel interference should have little influence on the values of $C_{m\,0}$ that would be obtained with a cambered model.

6.3. *Drag.* The variation of drag with lift is shown in Fig. 4 and with Mach number in Fig. 6. Most of the discussion below is based on the results at zero lift.

The difference between the measured values of $C_{D\,0}$ for the two models is seen from Fig. 4 to be between $0{\cdot}0015$ and $0{\cdot}0020$ at both the upper and lower ends of the test Mach number range. This is mostly due to the effect of Reynolds number on the skin-friction drag: theoretically, the difference in $C_{D\,0}$ should amount to about $0{\cdot}0011$. No firm explanation can be offered for the remainder of the measured difference but it was pointed out earlier that the absolute accuracy in C_D in any given test could be of the order of $\pm\, 0{\cdot}0005$. In order to study the tunnel-interference effects on $C_{D\,0}$, it was thought best to consider the variation of C_D for each model from the value at $M = 0{\cdot}8$. To the first order, this eliminates the effect of the different skin-friction drags and also, as quoted before, the variation of $C_{D\,0}$ with Mach number for either model should be accurate to $\pm\, 0{\cdot}0002$ in C_D.

This revised comparison of the variation of $C_{D\,0}$ with M for the two models is shown in Fig. 6. For both models, $C_{D\,0}$ increases by about $0{\cdot}002$ between $M = 0{\cdot}8$ and $M = 1{\cdot}19$, but whereas the whole increase for the small model occurs between $M = 0{\cdot}99$ and $1{\cdot}01$, the large model gives a

more gradual rise spread between $M = 0{\cdot}99$ and $1{\cdot}07$. The drag then overshoots by $0{\cdot}001$ in C_{D0} at $M = 1{\cdot}10$ before settling back by $M = 1{\cdot}19$ to the same value as for the small model. It could be added that the single high test point for the large model at $M = 1{\cdot}10$ was supported by the evidence from the earlier tests in which transition was not properly fixed. One can therefore be fairly confident that the curve is broadly as drawn in Fig. 6. In retrospect it would have helped if the tests had been made at closer intervals of Mach number in the region of $M = 1{\cdot}10$.

Analysis of the pressure-plotting results to be discussed below shows that the different variation in C_{D0} with M between $M = 0{\cdot}99$ and $1{\cdot}19$ is due mainly to wave-reflection effects on the large model and to a small extent, to the delayed movement of the terminal shock with this model. Similar results have been found on other models, but since the reflected disturbances may differ from model to model, the false peak in C_{D0} need not necessarily occur at $M = 1{\cdot}10$.

No mention has been made above of any blockage effect on C_D. This is because for these models, the start of the drag rise does not occur till very close to $M = 1{\cdot}0$ and so wave-reflection effects have the major influence. At subsonic speeds, prior to the start of the steep drag rise, C_{D0} would be expected to decrease slowly with Mach number because of the variation of the test Reynolds number, and hence the skin-friction drag, with Mach number. This trend is observed for the small model but not for the large model and so it would seem that the large model gives a tendency for an earlier drag rise with Mach number. This is the opposite of what one might expect on the basis of a simple blockage correction as derived from the lift data but the analysis of the pressure-plotting results in Section 7.1 below shows that the effect could be due to the apparent variation of blockage along the length of the model.

Apart from questions of tunnel interference, the values of C_D as measured by the balance can be affected by base pressure, the interference from the sting fairings and buoyancy. All the drag results presented here include a correction converting base pressure to free-stream static; this correction reaches a maximum of $0{\cdot}003$ in C_D supersonically. Because this correction has been applied, the drag comparison of the present models is not affected by the fact that the rapid change of base pressure when the terminal shock passes over the base, occurs at different Mach numbers for the two models (Fig. 7).

The sting fairing is a necessary source of interference on most slender-wing tests. The magnitude of the effect has been measured on some other models by supporting the model from below and pressure plotting the upper surface with and without a sting fairing in position. The correction has amounted to $0{\cdot}001$ in C_D at $M = 1{\cdot}4$ on a typical model. However, the present models both have similar fairings and so, even though the actual values of C_D may need correction for the presence of these fairings, the comparison as regards tunnel-interference effects should not be invalidated.

A buoyancy correction must be calculated for any particular model and as stated in Section 5.4 can be of the order of $0{\cdot}0002$ in C_D for a typical wing at $M = 1{\cdot}4$. It should be negligible below $M = 1{\cdot}2$.

So far, the discussion has merely concerned the drag at zero lift. The variation of $(C_D - C_L^2/\pi A)$ with C_L for different Mach numbers for the two models is plotted in Fig. 4 and also, the variation with Mach number in the drag increment between $C_L = 0$ and $C_L = 0{\cdot}1$ and $0{\cdot}2$ respectively is shown in Fig. 6. Any asymmetry in the curves of $(C_D - C_L^2/\pi A)$ is due mostly to the effects of tunnel upwash and would normally be eliminated by testing the model both erect and inverted. With regard to the curves of $(C_D - C_L^2/\pi A - C_{D0})$ in Fig. 6, it should be emphasised that agreement between the curves for the two models would mean that there are no Reynolds number effects

and that the tunnel-interference effects are not dependent on C_L; it would *not* mean that there are no tunnel-interference effects but that the tunnel-interference effects remain as shown by the C_{D0} curve.

For Mach numbers up to about $M = 1{\cdot}04$, the large model has more drag at a given lift such as $C_L = 0{\cdot}1$ or $0{\cdot}2$. This can be related to the better lift-curve slope on the small model which as mentioned earlier, is due to the fact that at the lower test Reynolds number with the smaller model, the leading-edge vortex develops at a lower incidence. This Reynolds number effect on lift-curve slope is not present at supersonic speeds and this is presumably why, for Mach numbers greater than $M = 1{\cdot}14$, the drag due to lift is much the same on the two models. In a small range of Mach number near $M = 1{\cdot}1$ however, the drag due to lift is smaller with the large model. As noted above, C_{D0} for the large model at $M = 1{\cdot}1$ is increased by wave-reflection effects and so the implication is that these wave-reflection effects decrease somewhat with increasing C_L, thus leading to too small a value for the drag due to lift. It will be shown later in Section 8 that the limited pressure-plotting data at incidence appears to confirm this suggestion.

7. *Pressure-Plotting Results and General Discussion.* The pressure-plotting results are shown as chordwise distributions of p/H for some Mach numbers near $M = 1{\cdot}0$ in Fig. 8 and as variations of p/H at particular hole positions with Mach number in Fig. 9. These figures primarily illustrate blockage effects. To show the effects of reflected waves, the variation of C_p with Mach number is given in Figs. 10 and 11 and chordwise distributions of C_p over the whole Mach number range are shown in Figs. 12 and 13. All these results are for zero incidence. The variation of p/H with incidence at $M = 0{\cdot}98$ and $1{\cdot}06$ appears in Fig. 14.

7.1. *Blockage.* Comparison of the chordwise distributions of p/H for the two models near $M = 1$ shows therefore the different blockage effects. These can be seen most clearly from Fig. 8b which compares the distributions for the small model at $M = 0{\cdot}99$ with the distributions for the large model at various related Mach numbers. Clearly, the agreement between the results for the two models at the same nominal Mach number is poor since for both spanwise stations ($\eta = 0{\cdot}25$ and $0{\cdot}45$) the distributions for the larger model show significantly lower suctions. To produce suctions of the same order as on the small model at $M = 0{\cdot}99$, the tunnel Mach number must be increased with the large model to between $M = 1{\cdot}00$ and $1{\cdot}01$. Thus there is a difference in blockage between the models of about $0{\cdot}015$ in M. Similarly Fig. 8a shows that $M = 0{\cdot}98$ for the small model is comparable with $M = 0{\cdot}99$ for the large model and Fig. 8c shows that two other comparable Mach numbers are $1{\cdot}00$ and $1{\cdot}02$. In the latter case however, the distribution is appreciably affected by reflected-wave interference and the comparison does not merely show blockage effects. From these figures therefore, it appears that average values for the differences in blockage between the two models are about $\Delta M = 0{\cdot}01$ when the large model is tested at an uncorrected Mach number of $0{\cdot}98$ and $\Delta M = 0{\cdot}015$ when it is tested at $M = 0{\cdot}99$ and probably $M = 1{\cdot}00$ also.

These average values are not however the end of the story. There are significant local variations along the chord of the models (in passing, it should be noted that near the leading edge, the pressure measurements may be influenced by the local roughness band which extends streamwise about $0{\cdot}05c_0$ from the leading edge, but the presence of these extraneous effects does not affect the general discussion). It appears that the blockage corrections vary with chordwise position both as regards their magnitude and as regards the Mach number at which they first become significant.

To see this in detail, it is best to refer to the comparison of p/H values at particular points on the two models as shown in Fig. 9a for the station at $\eta = 0{\cdot}25$ and Fig. 9b for $\eta = 0{\cdot}45$. Although these curves are drawn for Mach numbers above and below $M = 1{\cdot}0$, they only strictly show blockage effects for $M < 1{\cdot}0$ since reflected-wave interference occurs above this. It can be seen that the difference in blockage between the models for $M_{\text{uncorrected}} = 1{\cdot}0$ is given by $\Delta M = 0{\cdot}017$ for the $0{\cdot}4c_0$ position but is only $\Delta M = 0{\cdot}010$ at $0{\cdot}8c_0$. The present pressure-plotting results provide no data for points forward of $0{\cdot}4c_0$ but the evidence from the models of Ref. 4 shows that the blockage could be near zero at the nose of a model and only become significant further aft. Indeed, Ref. 4 tended to suggest that this could be a monotonic trend with the largest blockage at the rear which is not what was found in the present tests. However the results for the models of Ref. 4 show that a strong adverse pressure gradient, *i.e.*, the terminal shock for Mach numbers close to $M = 1{\cdot}0$, is present almost immediately downstream of the peak-suction (and maximum-thickness) position and so it is more plausible to interpret the apparently large blockage at the rear as a delay in the terminal-shock movement with Mach number which is rather more analogous to a reflected-wave effect. With the present models, the terminal shock is always some distance downstream of the maximum-thickness position and so it is possible to determine the trend in the blockage effect in this region. The combined results of all these tests show therefore that it is very likely that the local blockage near $M = 1{\cdot}0$ is at a maximum near the centre of a model or near its maximum thickness and that it becomes less towards either the nose or the trailing edge.

The other feature in the chordwise variation of blockage effect can also be seen in Fig. 9. This concerns the Mach number at which a local blockage effect first becomes significant. At $0{\cdot}8c_0$ at both spanwise positions, there is no sign of a blockage effect below $M = 0{\cdot}975$, whereas at $0{\cdot}67c_0$ it appears at about $M = 0{\cdot}96$. Further forward, the trends are not so clear but it seems that at $0{\cdot}4c_0$, it probably appears before $M = 0{\cdot}94$, *i.e.*, outside the range for which pressure-plotting data are available.

These chordwise variations of local blockage could explain several features in the blockage effects on the overall measurements. With regard to lift, it was seen that the blockage difference between the models began to show at about $M = 0{\cdot}93$ and this could be related to the suggestions made above that over the forward part of the wing, blockage effects are beginning to appear below $M = 0{\cdot}94$. There is still however a little apparent discrepancy nearer $M = 1{\cdot}0$ in that the pressure-plotting measurements do not anywhere suggest a blockage correction greater than about $0{\cdot}017$ and hence a mean correction less than this, whereas the lift-curve slope data suggested a figure of $0{\cdot}02$.

In the case of pitching moment, it was noted that there was no apparent effect of blockage on the aerodynamic-centre position and this can also be related as follows to the chordwise variations of local blockage noted above. In the absence of tunnel interference, the transonic rearward movement of aerodynamic centre is due to the change in chordwise loading. Now, if in the tunnel tests, blockage first appears near the nose and only later further aft, this would also result in the centre of load being further aft at any given free-stream Mach number. This effect of the chordwise variation of blockage could coincidentally compensate for the effect of the mean blockage in delaying the true aerodynamic-centre shift with Mach number. This could account for the apparent lack of a blockage correction on the aerodynamic-centre results which as noted earlier was observed not merely in the present tests but also in the results for the swept-wing-body models of Ref. 1.

A further contributory factor could be that since the maximum local blockage occurs near the centre of the model, it is less likely to affect the aerodynamic centre than if it were large near the

root and tail. On the other hand, a possible alternative explanation that the blockage corrections vary with incidence is *not* borne out by the experimental results for $M = 0{\cdot}98$ (Fig. 14 and Section 8). Hence it seems likely that the chordwise variation of blockage effect is the major factor.

Considering finally the possible effects of blockage interference on drag, it has already been stated that since the main transonic drag rise occurs near $M = 1{\cdot}0$, the reflected-wave interference is much more significant than blockage. However, the chordwise variations of local blockage could give rise to effectively a buoyancy correction and this could explain the tendency for a slow drag rise to appear on the larger model. It should be noted that for other models where the drag rise was occurring definitely before $M = 1{\cdot}0$, this effect of the chordwise variation of local blockage would probably be swamped by the effect of the mean blockage correction and so as with the results of Ref. 1, one would normally find that the drag rise was somewhat *delayed* with large models.

In all the discussions so far, the values quoted for ΔM have related to the difference in blockage between the large and small models. One is of course really interested in the absolute magnitude of the blockage corrections for any given model. This is not a trivial distinction because the discussion in Refs. 3 and 5 show that blockage can be quite significant for even a very small model. Theoretical expressions for blockage corrections have been given by Berndt for slotted-wall tunnels, Ref. 2, and Page for perforated-wall tunnels, Refs. 3, 4.

Page's theory has been applied to perforated-wall tunnels at National Aeronautics and Space Administration, Ames which have similar characteristics to the A.R.A. tunnel. For a body of revolution his expression is

$$\Delta M = -0{\cdot}82 \left(\frac{r^*}{R}\right)^{6/7} \left(\frac{r^*}{x^*}\right)^{2/7}$$

where x^* and r^* are the body co-ordinates at the forward sonic point.

R is the radius of a circular tunnel having the same cross-section area as the A.R.A. tunnel.

ΔM is the correction to be applied to the apparent Mach number and hence the negative sign in the above expression is quite consistent with the experimental data analysed so far. In applying this expression to the present models, there is some uncertainty because the position of the forward sonic point cannot be determined from the pressure-plotting data. As the sonic point moves rearward the formula gives increasing values of the blockage. Thus, assuming the sonic point is at $x^* = 0{\cdot}05c_0$, the blockage corrections are $\Delta M = -0{\cdot}005$ and $-0{\cdot}013$ for the small and large models respectively and for $x^* = 0{\cdot}15c_0$, they become $\Delta M = -0{\cdot}013$ and $-0{\cdot}033$. The sonic point should lie between these positions so that the difference in blockage corrections between the two models would be between $\Delta M = -0{\cdot}008$ and $-0{\cdot}020$. This offers reasonable agreement with the pressure-plotting results which show a mean difference in blockage between the models of $\Delta M = -0{\cdot}015$.

If we conclude therefore that the difference in blockage between the two models is given as $\Delta M = 0{\cdot}015$, this means that the absolute overall blockages for the two models at $M = 1{\cdot}0$ are about $0{\cdot}025$ and $0{\cdot}010$ in ΔM. Maximum local blockage effects near the maximum thickness are probably $\Delta M = 0{\cdot}030$ and $0{\cdot}012$.

It is very significant that the blockage only decreases from $0{\cdot}025$ to $0{\cdot}010$ in ΔM even though the blockage ratio based on cross-section area decreases from $0{\cdot}36$ to $0{\cdot}04$ per cent. Page's expression indicates that the blockage effect varies as the 6/7th power of the model dimensions and not as the square. Therefore reduction of model size may still leave a significant blockage effect, and also an increase in size may be tolerated without a severe increase in blockage penalty.

7.2. *Terminal-Shock Movement.* The results for the swept-wing models in Ref. 1 showed that one of the principal tunnel-interference effects near $M = 1{\cdot}0$ was a delay in the terminal-shock movement with Mach number. The existence of a similar effect with the present models is shown most clearly by Fig. 7 which compares the variation of base pressure with Mach number for the two models. The rise in pressure as the shock crosses the base occurs between $M = 1{\cdot}00$ and $1{\cdot}02$ for the small model and between $M = 1{\cdot}06$ and $1{\cdot}14$ for the large model. The base pressure results cannot however be used by themselves to obtain a quantitative idea of this interference effect because the base is not in the same position relative to the wing on the two models. On the large model, the base is 5 per cent of c_0 aft of the trailing edge while on the small model, it coincides with the trailing edge. One can however refer to Fig. 11 which indicates how the terminal shock passes points further forward on the large model. These curves, together with intermediate curves not shown, indicate that the shock passes $0{\cdot}9c_0$ at about $M = 1{\cdot}00$, $0{\cdot}95c_0$ at about $M = 1{\cdot}015$, $1{\cdot}0c_0$ at about $M = 1{\cdot}07$ and $1{\cdot}05c_0$ at about $M = 1{\cdot}10$. Thus in particular, it passes the trailing edge of the large model at about $M = 1{\cdot}07$ as compared with $M = 1{\cdot}01$ for the small model (*see* also the interpolated curve for the trailing-edge position in Fig. 7). In free-flight conditions, the terminal shock would be expected to reach the trailing edge at about $M = 1{\cdot}00$. It appears therefore that the small model shows very little delay in the movement of the shock, whereas with the large model there is a delay of about $0{\cdot}06$ to $0{\cdot}07$ in Mach number.

This delay in terminal-shock movement has some effect on the drag data in this Mach number range. Up to $M = 1{\cdot}07$, the large model has the terminal shock further upstream than it should be, and thus there is a region near the trailing edge where the pressures are too high. As a result, the measured drag is too low. A detailed analysis of the results suggests that this effect is less serious than the reflected-wave effects discussed below in Section 7.3, and so the delay in the terminal-shock movement is only partly the reason why the drag of the large model is too low at Mach numbers just above $M = 1{\cdot}00$*.

7.3. *Wave-Reflection Interference.* This type of interference was discussed in general terms in Section 5.2 and reference was made to the reflection properties of the tunnel as shown in Fig. 1d. The interference occurs in principle until all reflected waves have crossed the base *i.e.*, until $M = 1{\cdot}03$ for the small model and $M = 1{\cdot}26$ for the large model. The hope however is that over much of this range, the perforated walls will provide considerable alleviation of these reflected waves.

For the analysis of reflected-wave effects, C_p is a more suitable parameter than p/H since the effects of p/H tend to be overshadowed by its normal variation with Mach number. The reflected-wave effects are therefore shown most clearly by Figs. 10 and 11 which compare the variation of C_p with Mach number at particular pressure-plotting locations. Results are shown for both models but it should be noted that the actual chordwise positions of the pressure-plotting holes only coincide exactly at $x = 0{\cdot}4c_0$. Other results had to be interpolated and this was not easy since the effects are often quite localized. Above $M = 1{\cdot}03$, the small model should be free of tunnel interference and the results for this model are therefore a datum against which to judge wave reflections on the large model. One should not however attempt to put down every difference to

* It may be noted again that the drag values have been corrected for the difference in base pressure from free-stream static pressure and so they are not affected by the large change in base pressure as the terminal shock passes.

reflected waves. Above $M = 1{\cdot}10$, some of the differences between the results for the two models could be due to fluctuations in the empty-tunnel Mach number distribution along the centreline. This would particularly apply where the test Mach numbers did not coincide with the design Mach numbers at the end of the nozzle at the start of the tunnel working section. For example, the small model had to be tested at $M = 1{\cdot}41$ rather than $M = 1{\cdot}40$; also, it is thought that in this case some condensation shocks were present.

Despite these reservations, the comparisons in Figs. 10 and 11 should be quite satisfactory in showing the important reflected waves on the large model. It is found that the most conspicuous disturbances are the reflections of the bow shock and main expansion region. Owing to the model being at different distances from the tunnel walls, each incident wave system causes two reflected systems depending upon whether the reflections are from the top wall or from the floor and side walls. Using the notation of Ref. 1 the two reflections of the bow shock are referred to as A_T and A_S respectively, and analysis shows that the incident disturbances must originate at $0{\cdot}02c_0$ ahead of the apex.

On Fig. 10 at $0{\cdot}25$ semi-span, both reflections can be traced moving rearwards with increasing Mach number. For example, they cross the $x = 0{\cdot}4c_0$ position at about $M = 1{\cdot}03$ and $1{\cdot}06$. At $x = 0{\cdot}7c_0$, A_S is seen to cross at $M = 1{\cdot}07$ but A_T crosses at $M = 1{\cdot}14$, and Fig. 1d shows that the perforated walls should cancel the bow shock at this Mach number. In fact it can still be detected and so is not completely cancelled, but is of a much smaller magnitude. At higher Mach numbers, the bow shock meets the roof where the walls are too closed and it is reflected as a shock, *e.g.*, at $M = 1{\cdot}26$, $x = 0{\cdot}98c_0$. At this position A_S does not show, partly because its main effect would occur at $M = 1{\cdot}17$ which was not tested, but also because in its turn it is then being largely cancelled by the correct wall porosity. These movements of the bow-shock reflections are confirmed by the pressures at $0{\cdot}45$ semi-span in Fig. 11.

A similar variation with Mach number and position occurs for the reflections of the main expansion D_S and D_T. These are found to originate from the region of $x = 0{\cdot}38c_0$ and are probably influenced by the forward parts of the sting fairing as well as the expansion over the wing itself. They are neither as large nor as definite as the reflections of the bow shock, but appear quite clearly on Figs. 10 and 11 at both the spanwise stations.

There is evidence of other reflections which are less easy to define. At $x = 0{\cdot}4c_0$ and $0{\cdot}55c_0$ at Mach numbers only just above $1{\cdot}0$ several disturbances are reflecting simultaneously onto the same position and they do not separate until higher Mach numbers and further aft on the model. However the disturbances marked on Figs. 10 and 11 are all confirmed by pressures at intermediate positions which are not presented here. One of these other pairs of reflections is termed B_S and B_T and appears to originate from a compression just forward of the main expansion D *i.e.*, from about $x = 0{\cdot}35c_0$. It is probably the mean effect of the forward compression in front of the leading edge. Owing to the high sweepback angle of the leading edge and the longitudinal spread of the compression in front of it, this is a rather diffuse reflection. However it assumes particular importance when it augments the bow-shock reflection in a case such as $x = 0{\cdot}7c_0$, $M = 1{\cdot}06$, and it probably has a more extended effect than indicated by the symbols B_S and B_T on Figs. 10 and 11.

Another pair of reflections apparently stems from a 'nose expansion' at the front of the sting fairing at $x = 0{\cdot}1c_0$. These are referred to as C_S and C_T and are again less conspicuous than the bow shock and main expansion reflections but they can be consistently traced on several of the distributions.

The reflection X, Y is different from the others in that it originates from a disturbance from the saw teeth on the tunnel floor, about $0{\cdot}5c_0$ ahead of the apex of the large model. It is reflected from the tunnel roof and finally clears the model base by about $M = 1{\cdot}24$. The geometry is such that the wall porosity where it strikes the roof is nearly correct to cancel it over most of the Mach number range. It is however very noticeable at Mach numbers between $1{\cdot}08$ and $1{\cdot}14$. The direct disturbance from the floor crosses the model above $M = 1{\cdot}14$ and is the expansion Z on Fig. 10a at $M = 1{\cdot}3$, $x = 0{\cdot}4c_0$.

The reflections are not so easy to distinguish on the small model since they quickly traverse its short length in the small range of Mach number up to $M = 1{\cdot}03$ and again near $M = 1{\cdot}10$ for the reflections of the tunnel-floor disturbance.

The resulting effects of all the reflections on the large model are best seen on the chordwise distributions on C_p in Figs. 12 and 13. They are shown for $M = 1{\cdot}04$ and above and in nearly all cases the small model results can be used as a datum. The maximum difference in C_p due to reflections is of the order of $0{\cdot}03$ to $0{\cdot}04$ and this corresponds to a difference in p/H of about $0{\cdot}012$.

Incident expansion waves reflecting as compressions are not very significant: only in a few cases, is there a lower suction than on the smaller model *e.g.*, near the trailing edge at $M = 1{\cdot}04$. The really important reflections are undoubtedly the reflections of the bow shock A and forward compression B. These produce an extended region of over-expansion on the large model. This sometimes covers up to 50 per cent of the model length and gradually moves rearward with increasing Mach number. This region of over-expansion does not affect the lift and pitching moment since the disturbances are virtually the same on the upper and lower wing surfaces. However, it is the principal cause of the interference effects on C_{D0} that were seen in Fig. 6. The pressure distributions at $0{\cdot}25$ and $0{\cdot}45$ semi-span have been integrated to give drag and confirm the force measurements.

Up to about $M = 1{\cdot}06$ the region of high suction is primarily over the forward-facing areas of the wing and the drag is reduced. At higher Mach numbers it has moved aft and is mostly over rearward facing areas, and the drag is increased. A maximum drag increase occurs at $M = 1{\cdot}10$ when compressions C_S and D_T are at the trailing edge but the reflected-expansion region is influencing the whole of the rear of the model. At higher Mach numbers the expansion moves off the trailing edge and its magnitude is decreased by more suitable wall porosity, so the effect on drag is reduced and becomes negligible at $M = 1{\cdot}19$ and above. The expansion Z from the tunnel floor probably decreases the drag at Mach numbers up to $1{\cdot}19$ and has little effect between $1{\cdot}19$ and $1{\cdot}4$ since it lies near the centre of the model. If Mach numbers above $1{\cdot}4$ were tested it would lie over the rear of the model and increase the drag.

As mentioned already the terminal-shock movement is delayed by tunnel interference and it does not cross the trailing edge until after $M = 1{\cdot}06$. The chordwise pressure distributions show that although this also decreases drag the effect is small compared with that of reflected waves.

In making corrections to other slender-wing models it is considered important that the present models may not be representative, in that they have a round leading edge and a rather bluff nose to the sting fairing which is effectively a fuselage. Thus the two strong compressive fields A and B may be exaggerated on these models, and when reflected give high suctions not representative of other geometries. Tests on other models are therefore assisted if some pressure plotting can be incorporated to measure the reflected interference or at least an estimate be made of the strength of the incident and reflected fields. It may also be an advantage to mount the models further forward in the tunnel so that incident fields are better cancelled by the correct wall porosity (*see* Section 9.2.2.).

8. *Incidence Effects.* So far, only the pressures at zero incidence have been discussed. Pressure measurements at other incidences were only made at $M = 0{\cdot}98$ and $1{\cdot}06$.

The effects of incidence on the pressures are shown in Figs. 14 and 15a and b. Fig. 14 shows the variation of p/H with incidence at some particular points on the model at $0{\cdot}45$ semi-span. Results at $0{\cdot}25$ semi-span are similar and are not shown. The most noticeable effect evident at $M = 0{\cdot}98$ is not due to tunnel interference but to the difference in test Reynolds numbers for the two models. This concerns the vortex development from the rounded leading edge which occurs at a lower incidence on the small model at the lower Reynolds number. This is consistent with the comparison of the lift data in Fig. 2, which showed that the small model develops significantly more lift than the large model at incidences above about 4 deg for Mach numbers up to about $M = 1{\cdot}10$. No other marked effects of incidence can be seen in the pressure results for $M = 0{\cdot}98$. In view of the limited extent of the data, it would perhaps be unreasonable to expect to establish any correlation with what was said earlier about blockage effects (or the absence thereof) on overall lift and pitching moment. It is perhaps fair to comment however that none of the data analysed has suggested any variation in the blockage effects with incidence and hence there is no reason to withdraw from the explanations put forward in Section 7.1.

At $M = 1{\cdot}06$ however, the tunnel-interference effects appear to change appreciably with incidence. This is not very obvious in Fig. 14 but this is largely coincidental as can be seen from the comparison in Figs. 15a and b of the chordwise pressure distributions for the two models at $\eta = 0{\cdot}25$ and $0{\cdot}45$, and $\alpha = 0$ and 4 deg. It has already been noted that the higher suctions on the large model at about $x = 0{\cdot}6c_0$ at $\alpha = 0$ deg are due to reflections of the bow shock and forward compression region. Fig. 15 shows that these reflections evidently become weaker with increasing incidence. The reason for this is not clear: it could be at least partly due to a change in strength of the incident disturbances. These effects as observed in the pressure results are borne out by the overall drag data. As noted earlier, these wave-reflections result in an increase in C_{D0} for the large model near $M = 1{\cdot}10$. Referring to Fig. 6b, it is seen that the drag due to lift at $C_L = 0{\cdot}2$ is in fact less for the large model than for the small model at $M = 1{\cdot}06$ and $1{\cdot}10$. Thus the drag data also suggest that the wave-reflection interference, which causes the large model to have too high a drag at these Mach numbers, decreases somewhat with incidence. As a result, the measured drag due to lift for the large model in this Mach number range is too low.

9. *Concluding Remarks.* 9.1. *Principal Results for These Models.* The types of tunnel interference apparent on the present models are blockage, retarded terminal-shock movement and wave reflections.

Blockage effects occur on local pressures and on lift-curve slope. The tests show the comparative blockage effect between the large and small models and an estimate of this difference, based on a theory by Page, agrees quite well and enables absolute values to be obtained. For lift-curve slope these values are $\Delta M = 0{\cdot}025$ and $0{\cdot}010$ for the large and small models respectively, these being maximum values occurring at an apparent Mach number of unity, so that the effective Mach numbers are only $0{\cdot}975$ and $0{\cdot}99$. Maximum local blockage is possibly $\Delta M = 0{\cdot}030$ and $0{\cdot}012$ and occurs about half-way along the models. Evidence from pressure measurements in these and other tests indicates blockage is small near the nose and trailing edge. Blockage effects on lift-curve slope commence near $M = 0{\cdot}93$ and gradually increase to their maximum values at $M = 1{\cdot}00$. There is some indication that local blockage commences first over the front of the models and only

later at the rear. This variation of blockage along the model, both in magnitude and in commencement, is suggested as the reason for the absence of any blockage effect on the rearward movement of aerodynamic centre. It is noted that transonic tunnel tests on swept-wing models also showed a blockage effect on lift-curve slope but not on movement of aerodynamic centre. For the slender wings the drag rise is so near $M = 1{\cdot}0$ that it is not affected by blockage. The theory shows that the blockage correction varies as the 6/7th power of the model linear dimension, so that the percentage blockage ratio of a model in the tunnel is not a good criterion to judge the resulting blockage effects.

The rearward movement of the terminal shock is delayed so that it crosses the trailing edge at $M = 1{\cdot}07$ and $1{\cdot}01$ for the large and small models respectively. This decreases the drag in this Mach number range but by only a small amount in this particular case.

Regarding reflected-wave interference, the most serious disturbances are the reflections of the bow shock and forward compression region. Up to between $M = 1{\cdot}15$ and $1{\cdot}19$, these incident compression waves reflect as expansion waves and therefore increase the suctions over parts of the model surface. This does not materially affect lift and pitching moment but has a marked effect on drag. Instead of a rapid increase in C_{D0} between $M = 0{\cdot}99$ and $1{\cdot}01$, the reflected waves cause a slow drag rise between $M = 0{\cdot}99$ and $1{\cdot}07$ and then it overshoots to give at $M = 1{\cdot}10$ a maximum value that is about $0{\cdot}001$ too high in C_D. The drag is low when the reflections of the bow shock are affecting the forward part of the model and high when these reflections are crossing the rear of the model. There is some evidence to suggest that the reflections of the bow shock and the consequent effects on C_D become less serious with increasing C_L. This means that near $M = 1{\cdot}06 \sim 1{\cdot}10$, the results for the large model give too small a value for the drag due to lift.

Other reflected waves as well as a disturbance from the saw-tooth junction in the tunnel floor can also be detected from the pressure-plotting results, but their effects on the overall results are relatively minor, and even on the pressure-plotting data they can be removed fairly precisely.

9.2. *General significance of Results and Application to Other Slender-Wing Models.* 9.2.1. *Blockage effects.* The present tests have shown that the blockage correction on lift-curve slope at an uncorrected Mach number of $1{\cdot}00$ amounts to about $0{\cdot}025$ in M for a model having a blockage ratio of $0{\cdot}36$ per cent. Earlier tests on a swept-wing model with a blockage ratio of $0{\cdot}5$ per cent gave a correction of only about $0{\cdot}02$ in M, and hence the new results confirm the expectation that transonic interference for a given blockage ratio may be larger for slender models. The actual magnitude of the blockage correction is about the same or perhaps marginally greater than predicted by Page's formula. It seems therefore that it would be reasonable to use this formula for estimating the corrections for other slender-wing models. It should be noted that to use this formula, one needs to know the position of the forward sonic point and it is desirable to obtain some pressure-plotting data on different models to determine this more precisely.

The variation of the local blockage effects with chordwise position has been shown to be important. In particular, this could account for the fact that no blockage correction appears to be needed for aerodynamic-centre position and for the fact that with models having a drag-rise Mach number very close to $M = 1{\cdot}0$, a slow premature drag rise could be present for large models. It is possible that similar effects could exist with less slender models.

9.2.2. *Wave-reflection effects.* In the present tests, the reflections of the bow shock and forward compression region have a fairly major effect on the peak value of C_{D0}. It is probable however that the bow shock and incident waves are stronger for these models than for more typical slender-wing

designs now being tested. This is partly because the present models had rounded leading edges and also a relatively large body fairing. If this is true, this would have accentuated the effect of the reflected disturbance. Also, as illustrated in Fig. 1d, the perforated walls would have been more successful in alleviating these disturbances if the models had been placed further forward in the working section. This would have meant that the bow shock at low supersonic Mach numbers would have struck the wall where it was less open and therefore the reflection would have been weaker. In fact if the models had been say, 8 in. further forward, the improved reflected waves might have been relatively trivial for $M = 1 \cdot 1$ and above. One can therefore assert that tests on slender-wing models placed at the most suitable position in the tunnel should give reasonable interference-free results at Mach numbers from about $M = 1 \cdot 1$ upwards. Further, on the basis of the evidence presented in this note, it should be possible to devise corrections even in the range $M = 1 \cdot 0$ to $1 \cdot 1$ particularly if a few pressure-plotting points are included in the models under test so that one can track the passage of any reflected disturbances and of the terminal shock.

Finally, it is perhaps worth emphasising that there is no real conflict between the results of the present investigation and the results from the reflected-wave analysis for the swept-wing-body models of Ref. 1. At first sight, the conclusions appear to disagree because in the present report much emphasis has been placed on the reflections of the bow shock and forward compression region whereas in the analysis in Ref. 1, it was asserted that these are of relatively little significance as compared with the fact that the perforated walls do not cope so well in eliminating reflections of expansion fields. There are several reasons why there is no conflict here, *viz.*,

(1) reflections of expansion fields in the present case pass downstream of the wing trailing edge at a relatively low supersonic Mach number and hence are relatively less important,

(2) the present models were placed further aft in the tunnel and hence the longitudinal distribution of open-area ratio of the walls was less suited to the reflection requirements,

(3) for the swept-wing-body models of Ref. 1, reflections of the bow shock when they existed at low supersonic Mach numbers passed ahead of the wing leading edge and hence had relatively less effect on the overall C_D.

Acknowledgement. The authors wish to acknowledge the assistance of Mr. J. N. King who was mainly responsible for the execution of the tests and computing of the results analysed in this report.

LIST OF SYMBOLS

$\bar{\bar{c}}$	Aerodynamic mean chord
c_0	Centreline chord
C_L, C_D, C_m	Lift, drag and pitching-moment coefficients (reference $\bar{\bar{c}}$)
C_p	Pressure coefficient
p	Local static pressure
H	Total pressure
M	Mach number
R	Reynolds number
α	Incidence
η	Spanwise position (proportion of semi-span)
x	Distance from leading-edge apex

REFERENCES

No.	*Author*	*Title, etc.*
1	F. O'Hara, L. C. Squire and A. B. Haines	An investigation of interference effects on similar models of different size in various transonic tunnels in the U.K. A.R.A. Wind Tunnel Note 27. February, 1959. Unpublished M.o.A. Report.
2	S. B. Berndt	Theoretical aspects of the calibration of transonic test sections. F.F.A. Report No. 74. 1957.
3	W. A. Page	Experimental study of the equivalence of transonic flow about slender cone-cylinders of circular and elliptic cross section. N.A.C.A. Tech. Note 4233. April, 1958.
4	W. A. Page and J. R. Spreiter ..	Some application of transonic-flow theory to problems of wind-tunnel interference. A.G.A.R.D. Report 293. March, 1959.
5	A. B. Haines and J. C. M. Jones	The centre-line Mach-number distributions and auxiliary-suction requirements for the A.R.A. 9 ft × 8 ft Transonic Wind Tunnel. A.R.A. Report 2. A.R.C. R. & M. 3140. April, 1958.

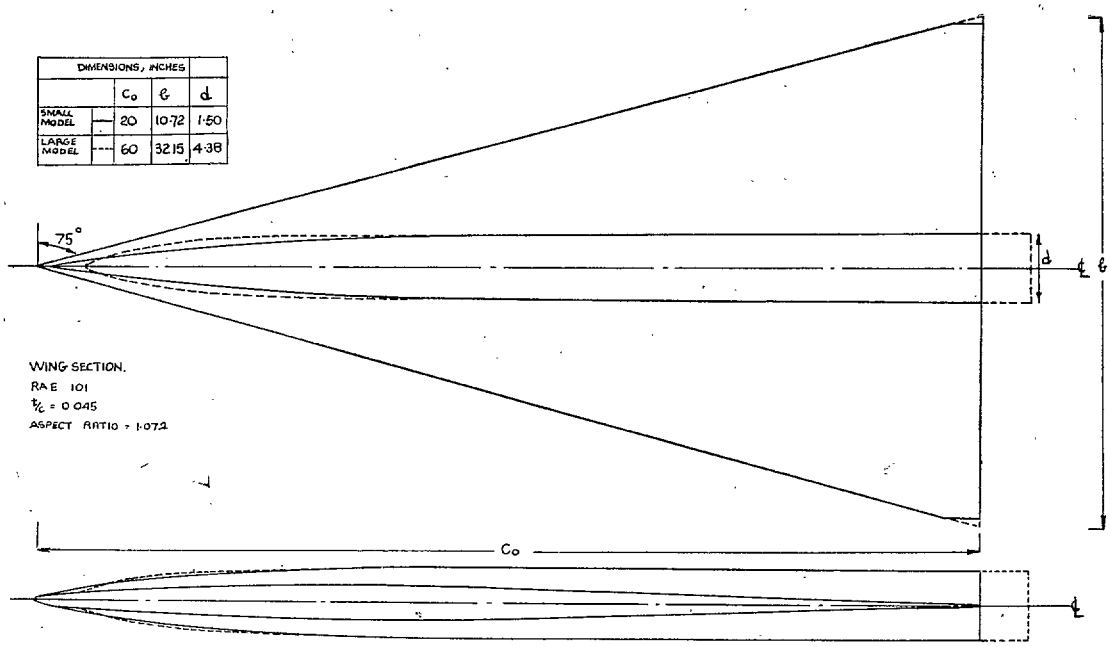

FIG. 1a. General arrangement of models.

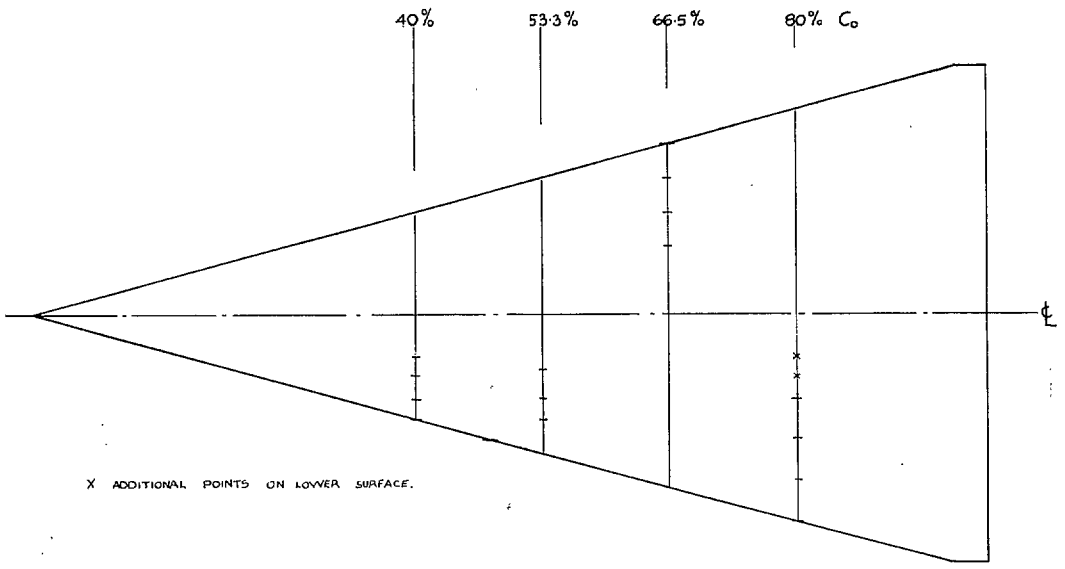

FIG. 1b. Upper-surface pressure-plotting points on small model.

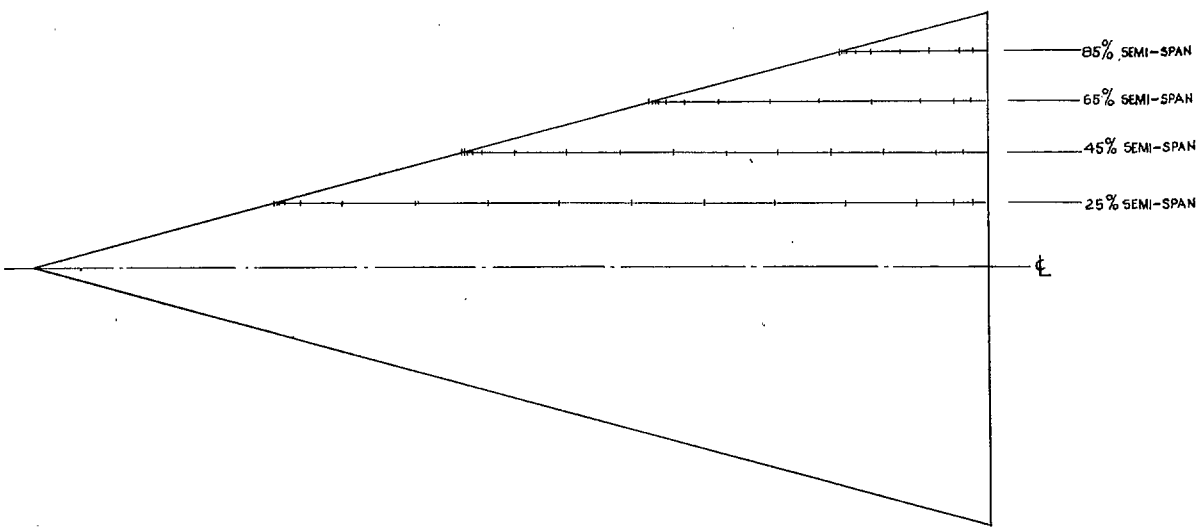

FIG. 1c. Upper-surface pressure-plotting points on large model.

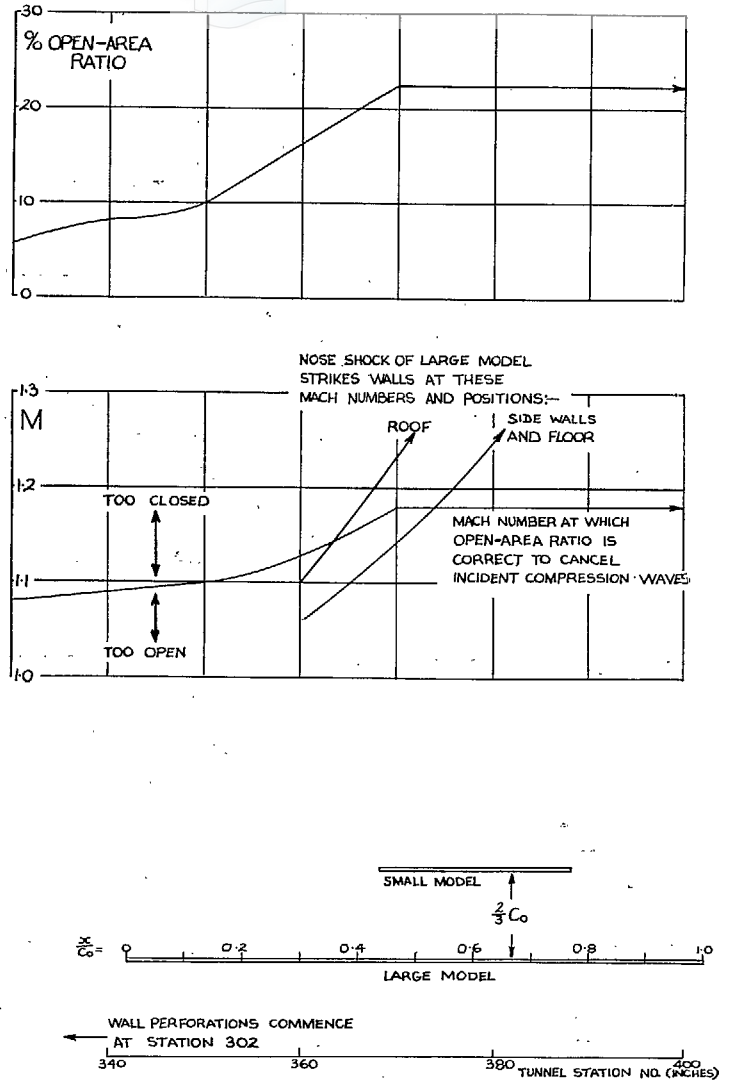

FIG. 1d. Longitudinal positions of models and properties of perforated walls.

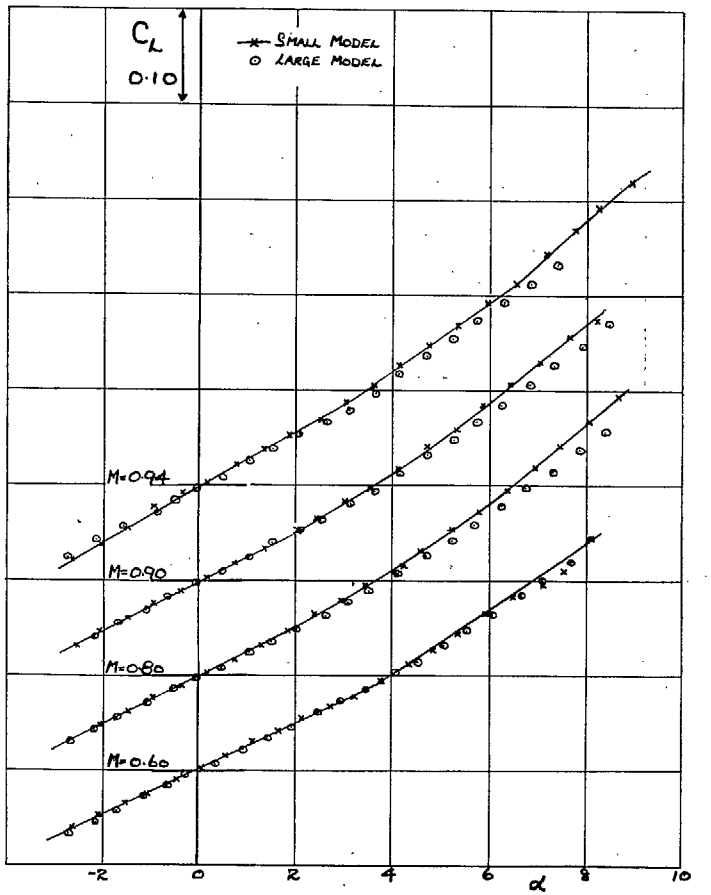

FIG. 2a. Lift curves. $M = 0{\cdot}60$ to $M = 0{\cdot}94$.

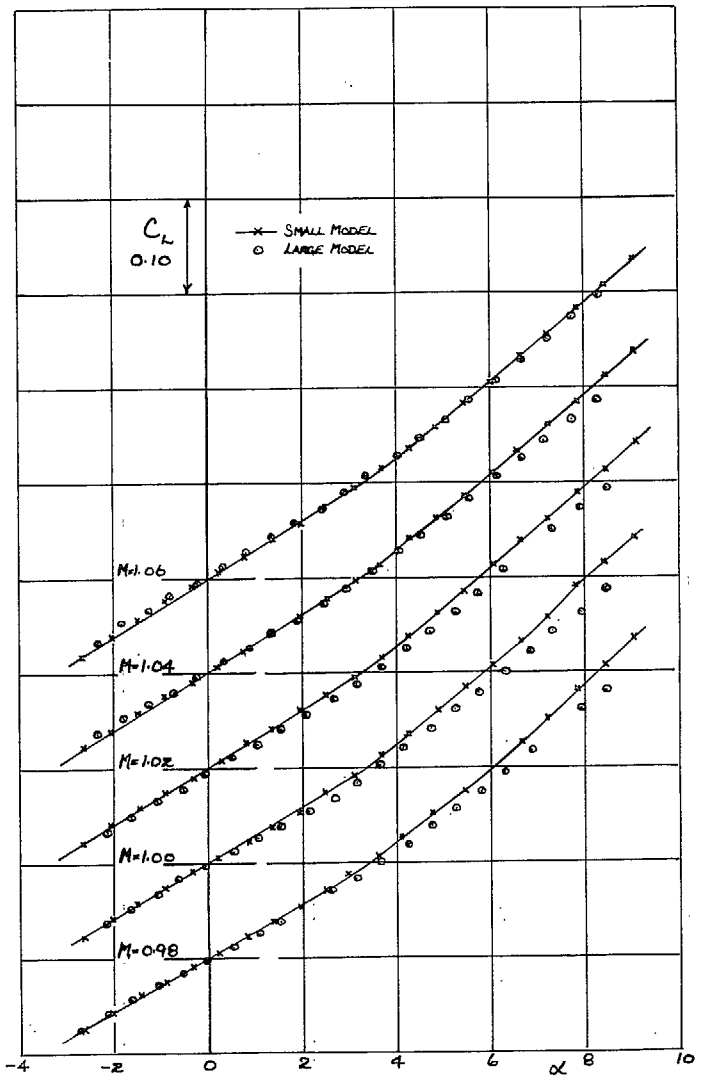

FIG. 2b. Lift curves. $M = 0{\cdot}98$ to $M = 1{\cdot}06$.

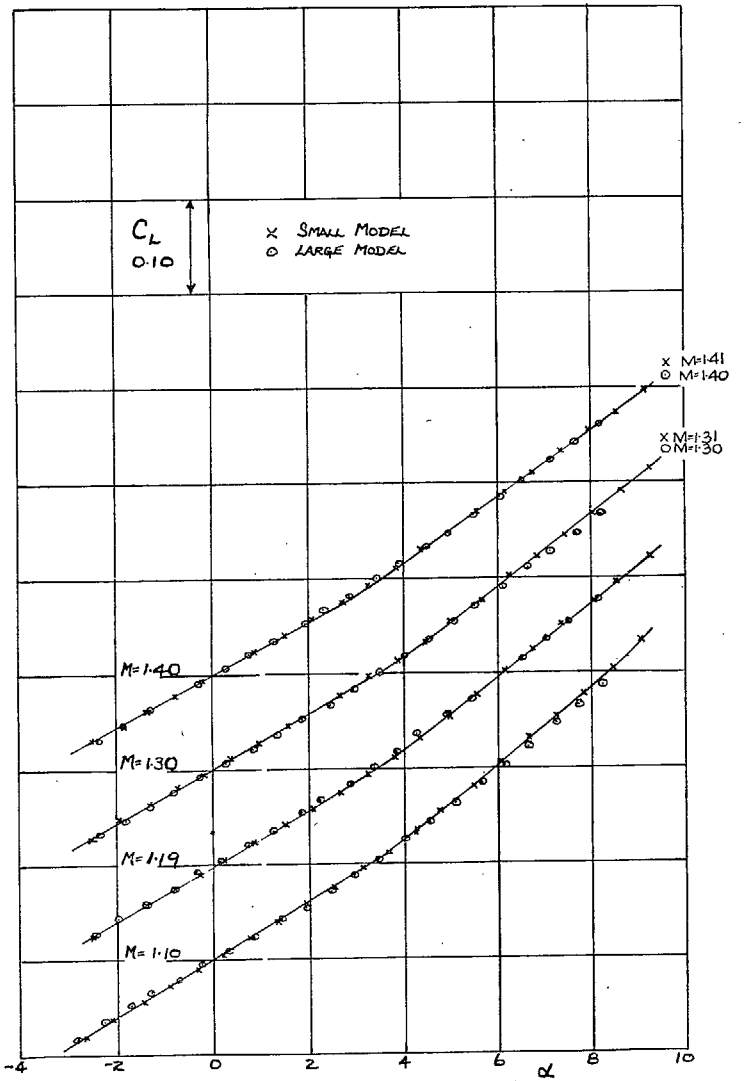

FIG. 2c. Lift curves. $M = 1{\cdot}1$ to $M = 1{\cdot}4$.

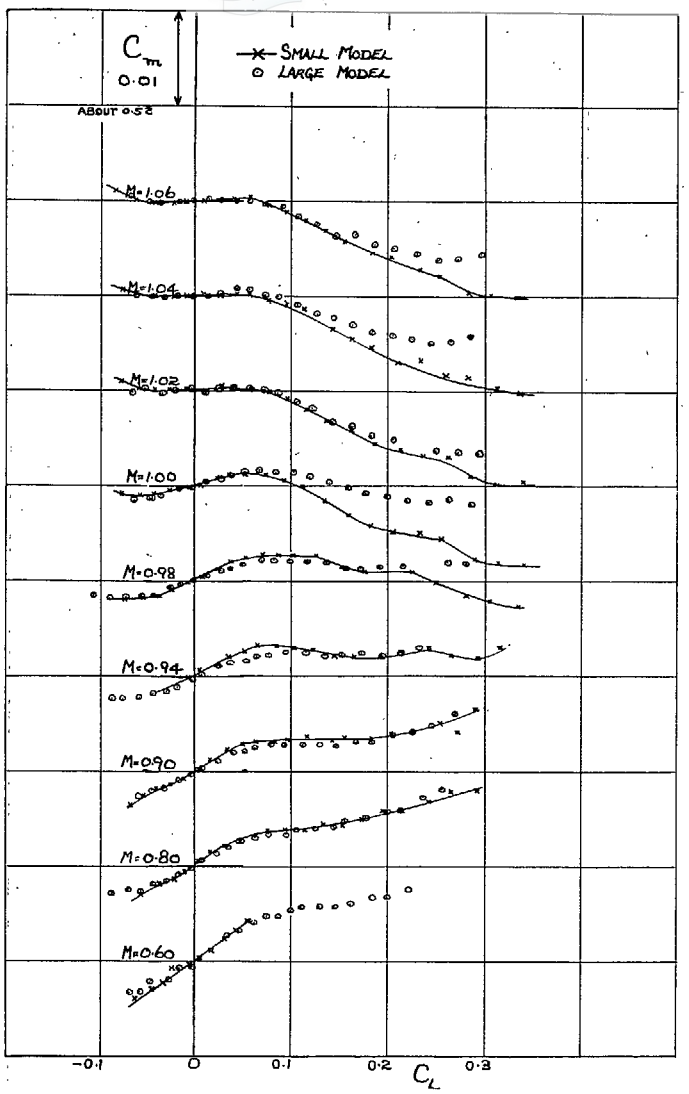

FIG. 3a. Pitching-moment curves. $M = 0{\cdot}60$ to $M = 1{\cdot}06$.

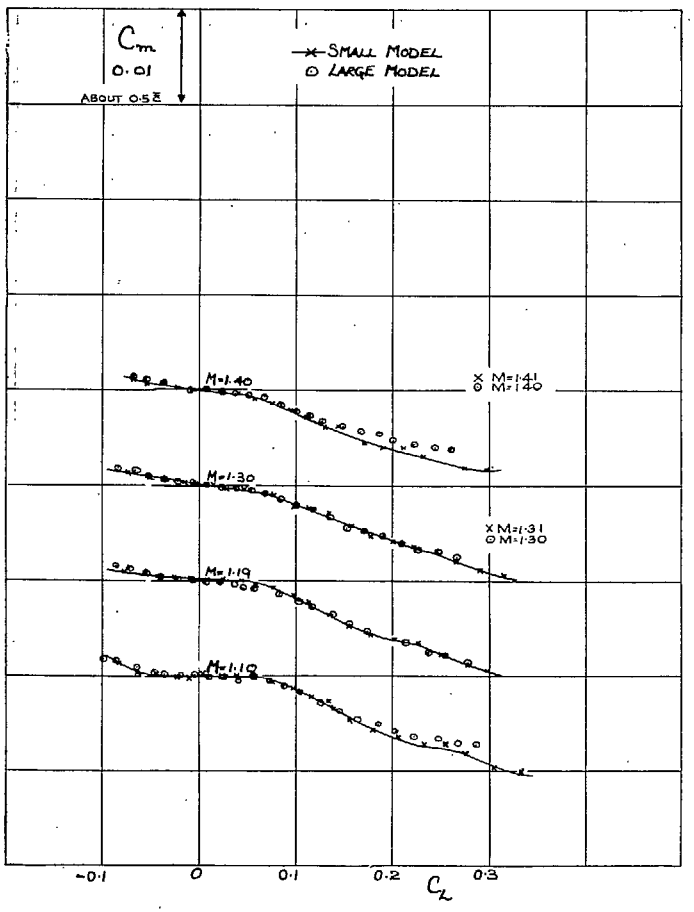

FIG. 3b. Pitching-moment curves. $M = 1{\cdot}1$ to $M = 1{\cdot}4$.

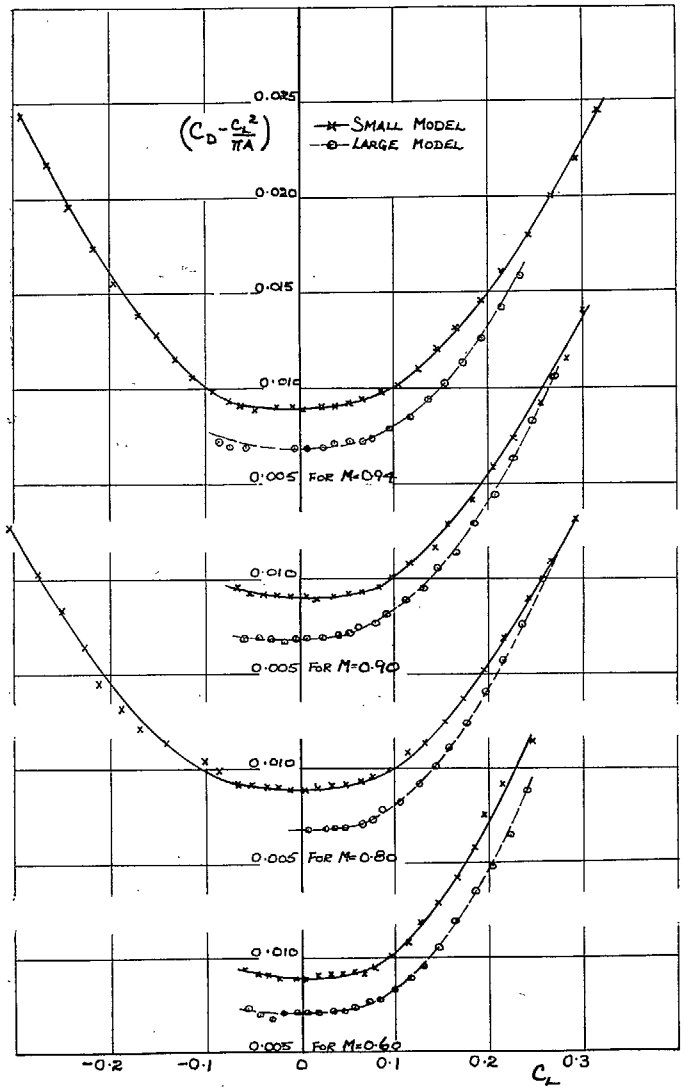

FIG. 4a. Variation of $(C_D - C_L^2/\pi A)$ with lift. $M = 0{\cdot}60$ to $M = 0{\cdot}94$.

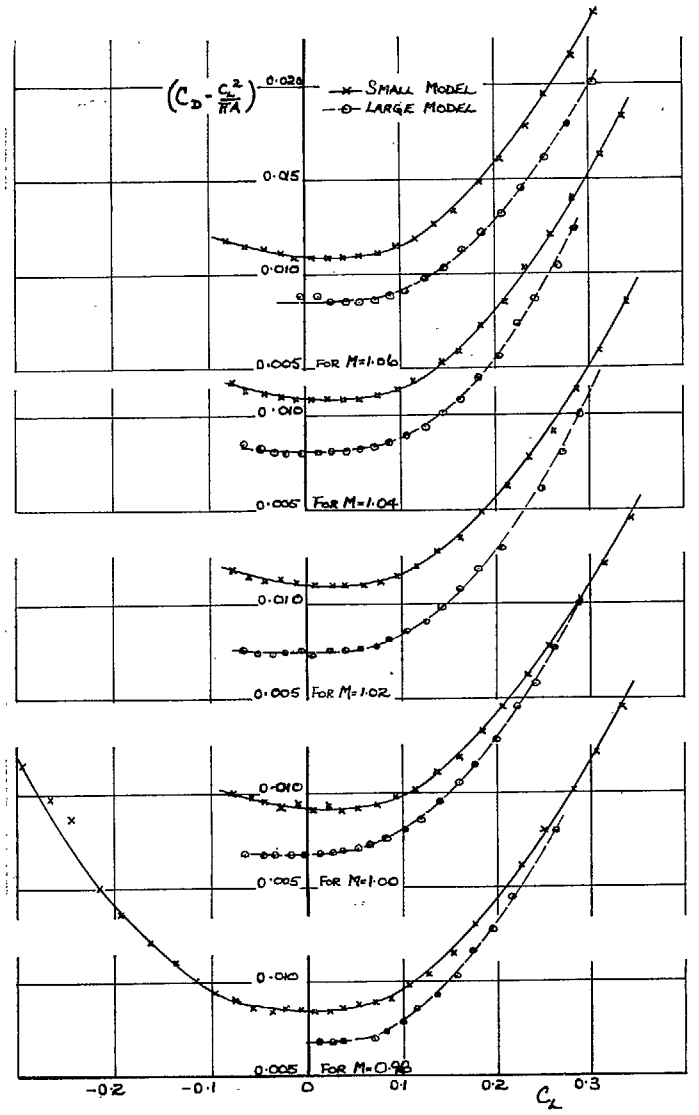

FIG. 4b. Variation of $(C_D - C_L^2/\pi A)$ with lift. $M = 0{\cdot}98$ to $M = 1{\cdot}06$.

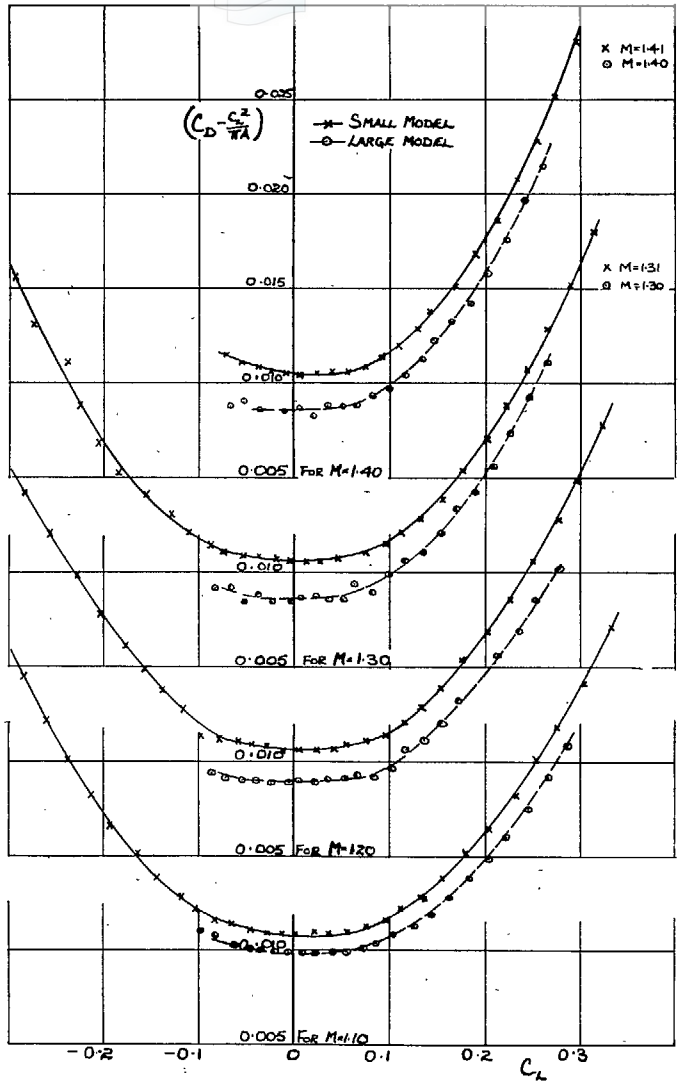

FIG. 4c. Variation of $(C_D - C_L^2/\pi A)$ with lift. $M = 1{\cdot}1$ to $M = 1{\cdot}4$.

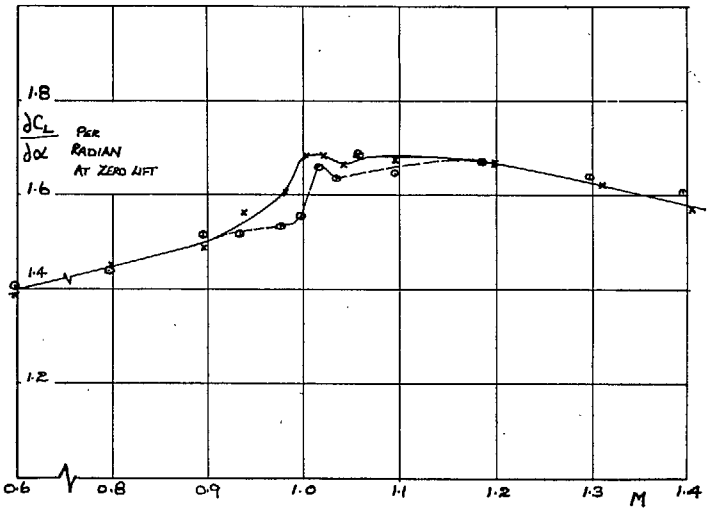

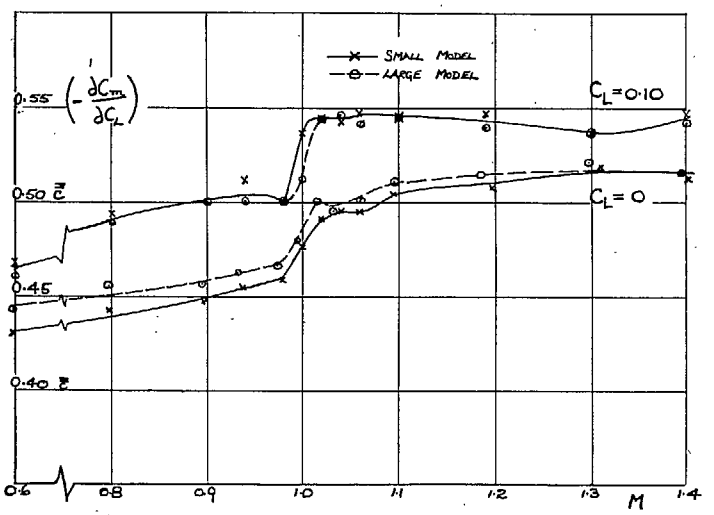

FIG. 5. Variation of lift-curve slope and aerodynamic-centre position with Mach number.

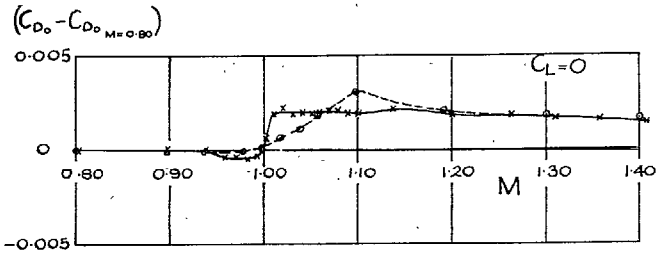

(a) ZERO-LIFT DRAG.

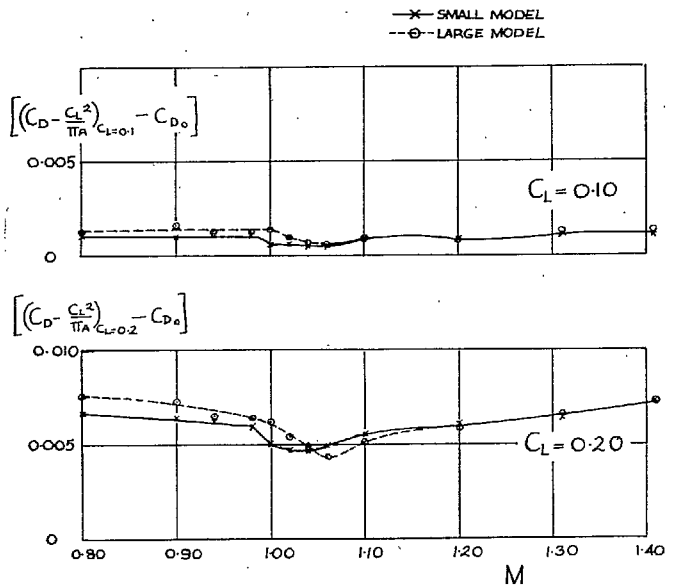

(b) DRAG DUE TO LIFT

FIGS. 6a and b. Variation of drag with Mach number.

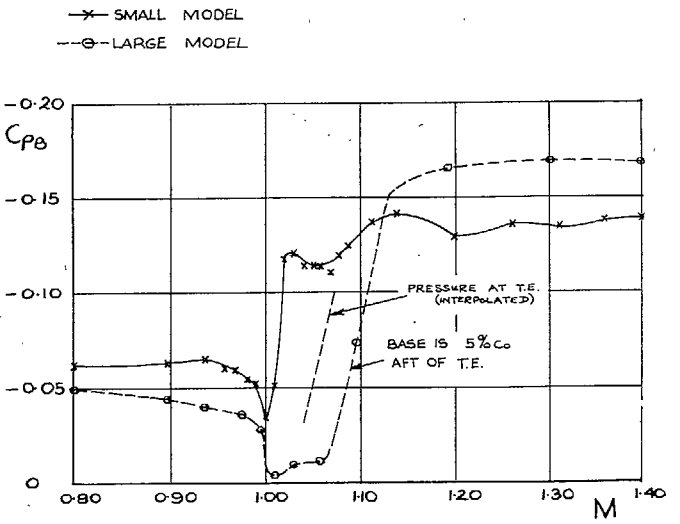

FIG. 7. Variation of base pressure with Mach number.

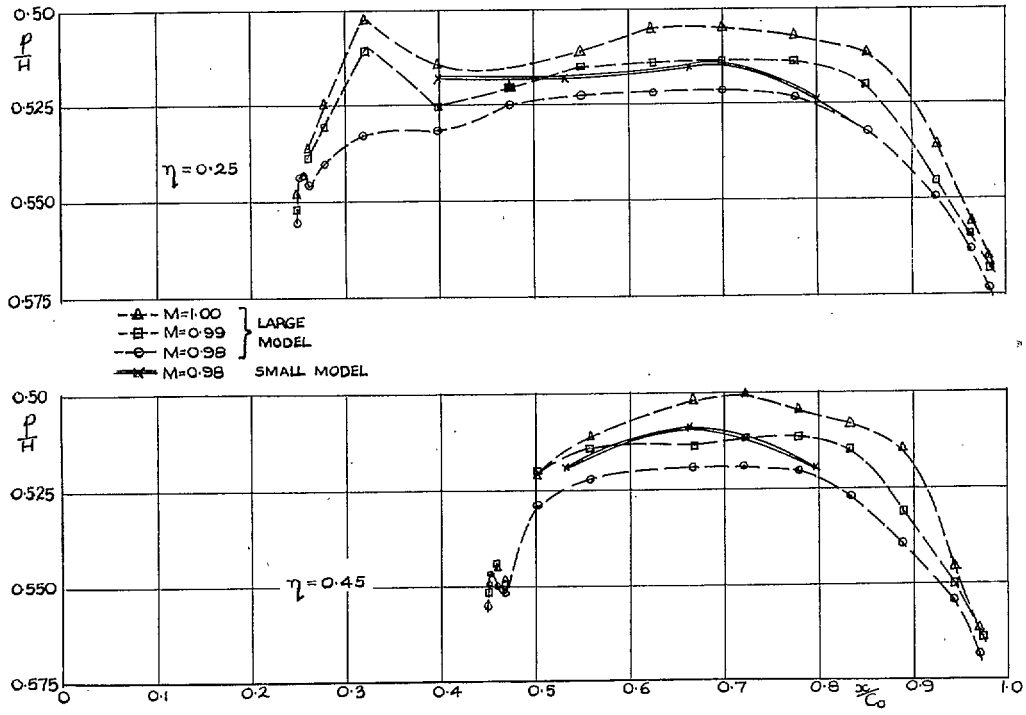

FIG. 8a. Chordwise pressure distribution. $M \geqslant 0{\cdot}98$.

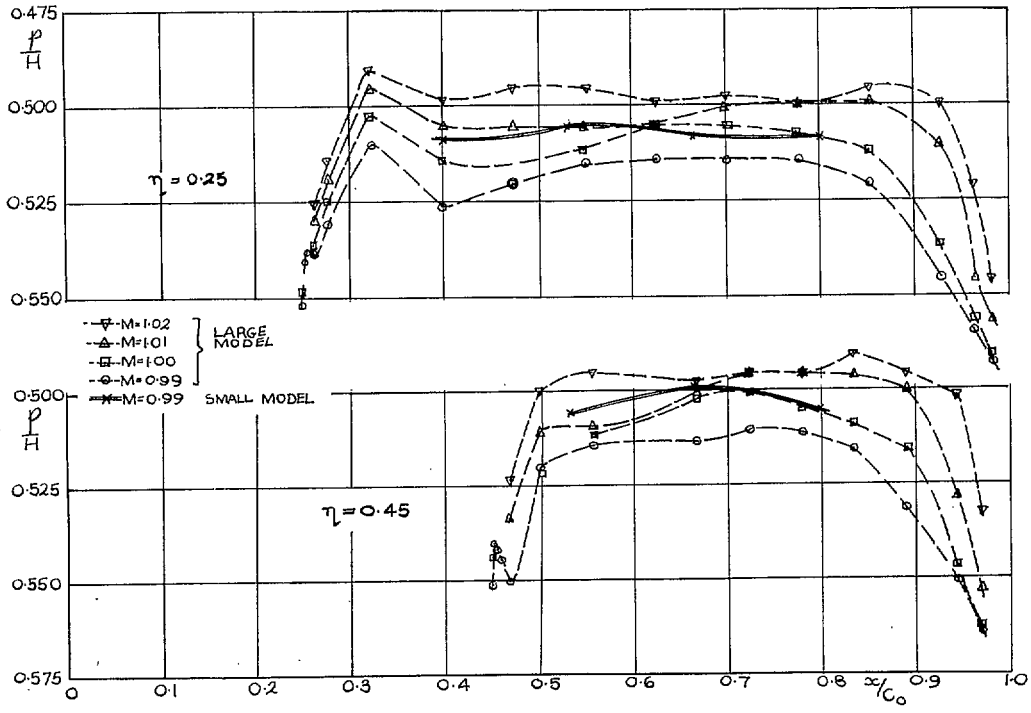

FIG. 8b. Chordwise pressure distribution. $M \geqslant 0{\cdot}99$.

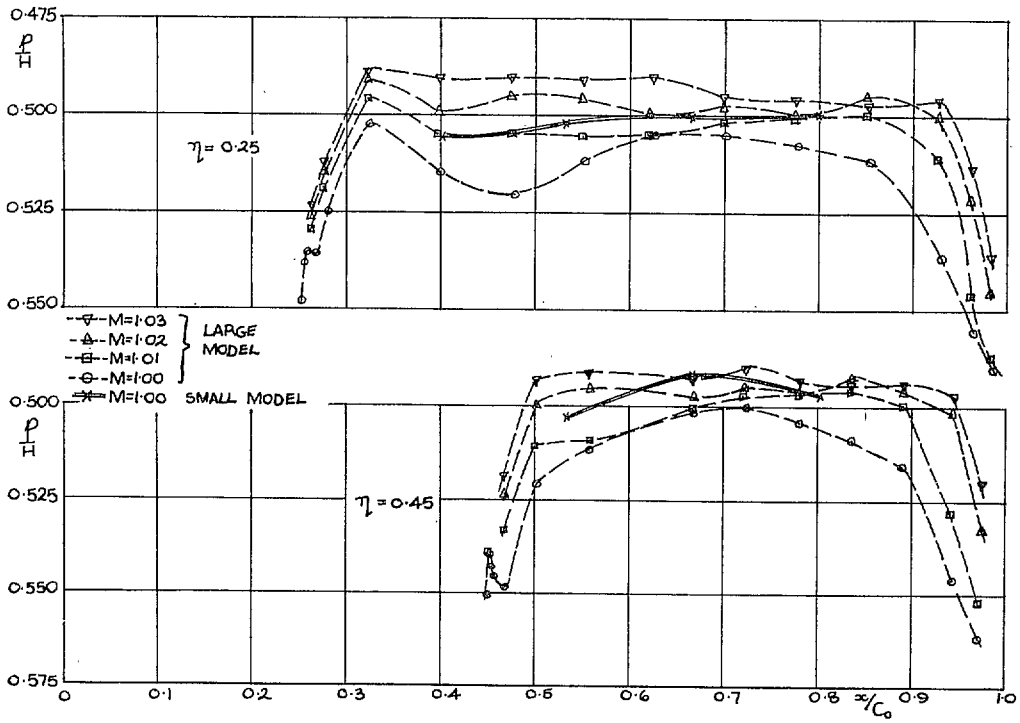

FIG. 8c. Chordwise pressure distribution. $M \geqslant 1{\cdot}00$.

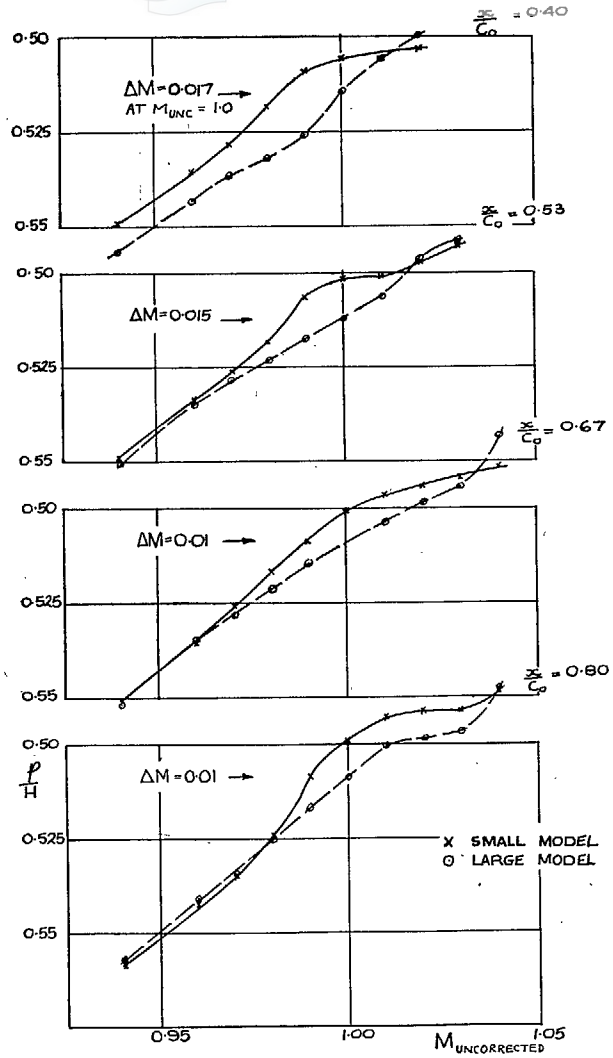

FIG. 9a. Variation of p/H with Mach number. $\eta = 0{\cdot}25$.

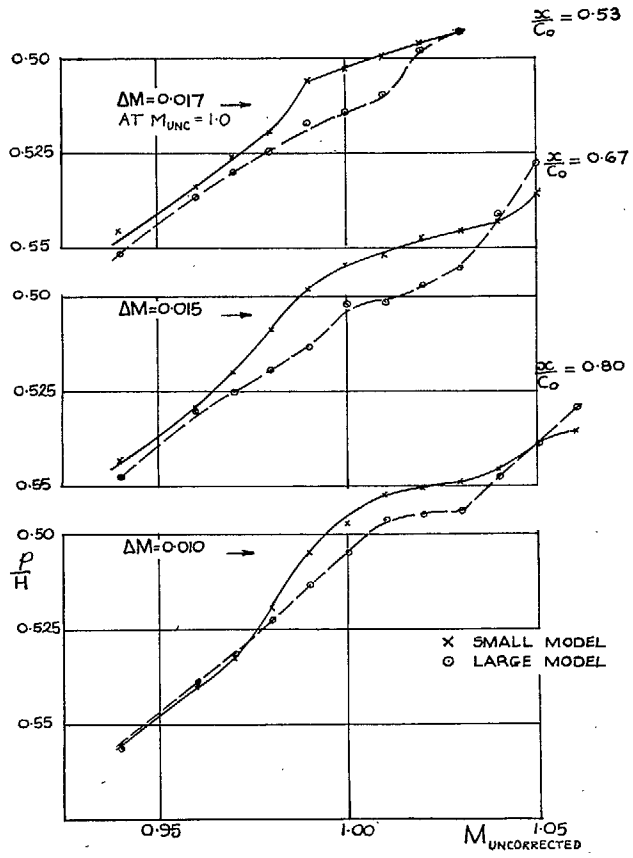

FIG. 9b. Variation of p/H with Mach number. $\eta = 0{\cdot}45$.

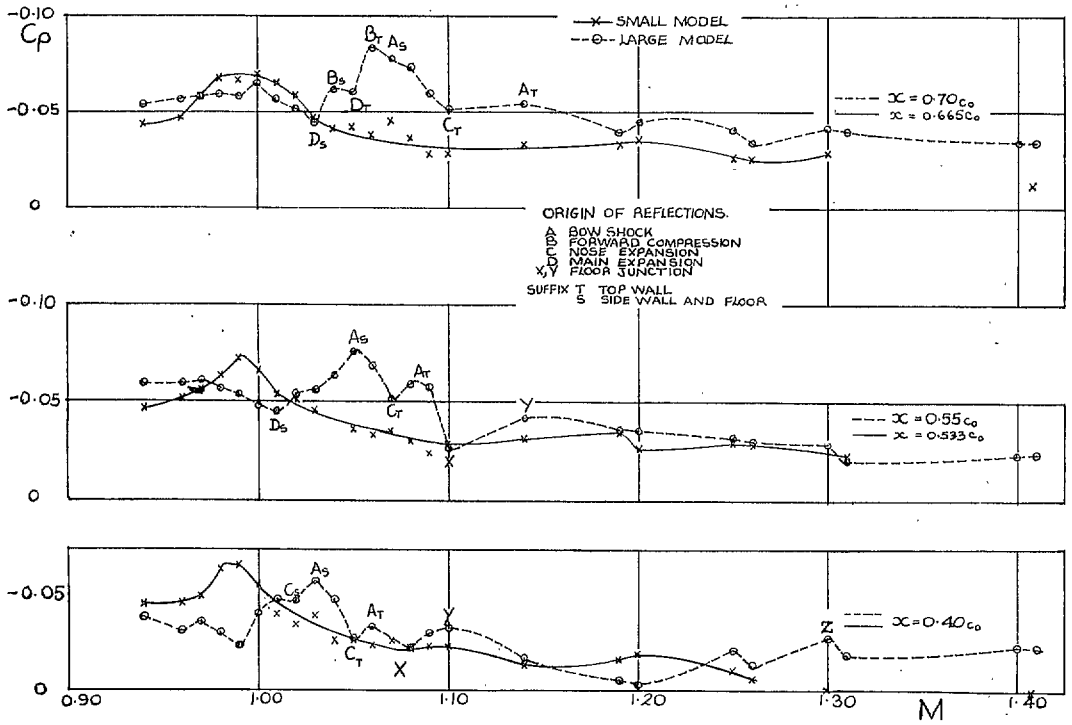

FIG. 10a. Variation of C_p with Mach number at particular points. $\eta = 0{\cdot}25$.

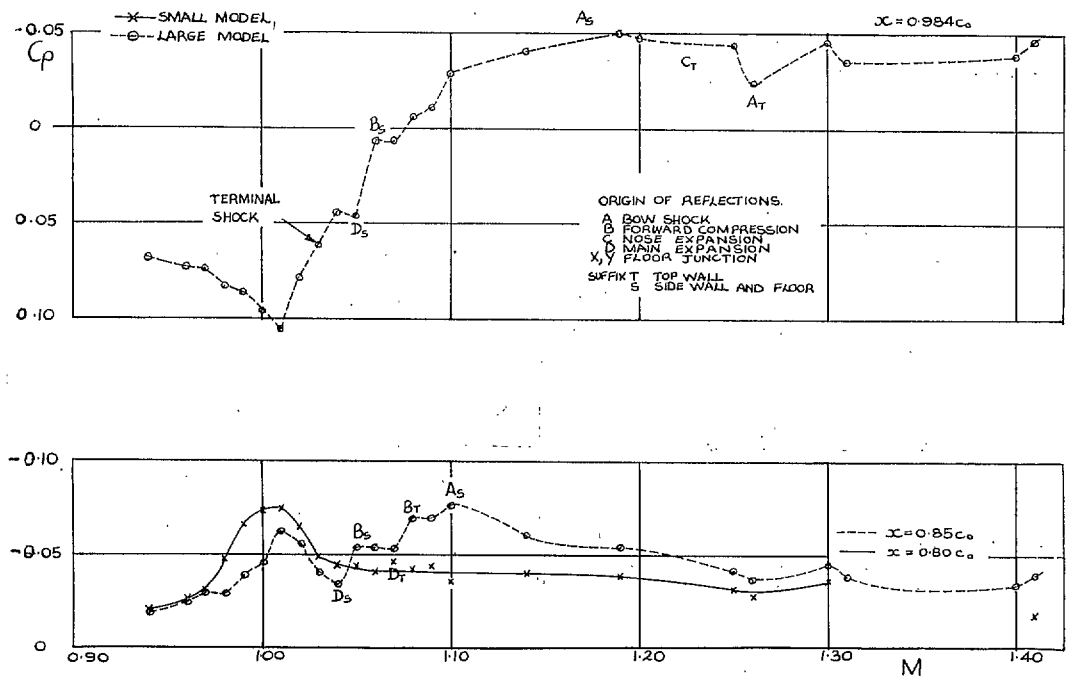

FIG. 10b. Variation of C_p with Mach number at particular points. $\eta = 0{\cdot}25$.

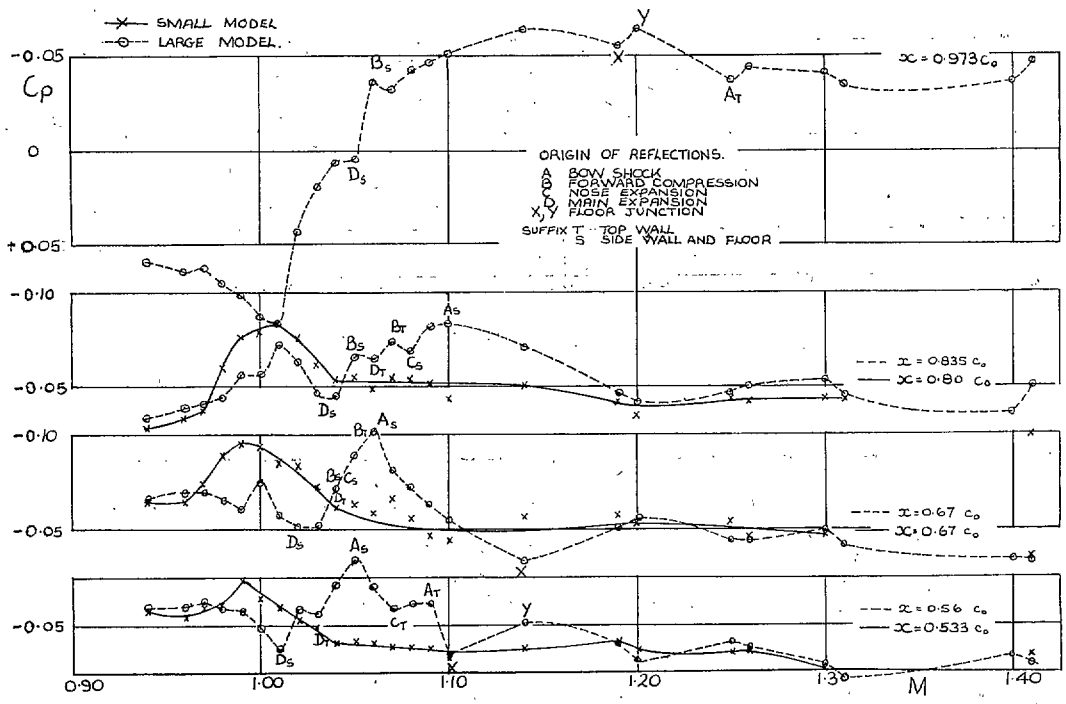

FIG. 11. Variation of C_p with Mach number at particular points. $\eta = 0{\cdot}45$.

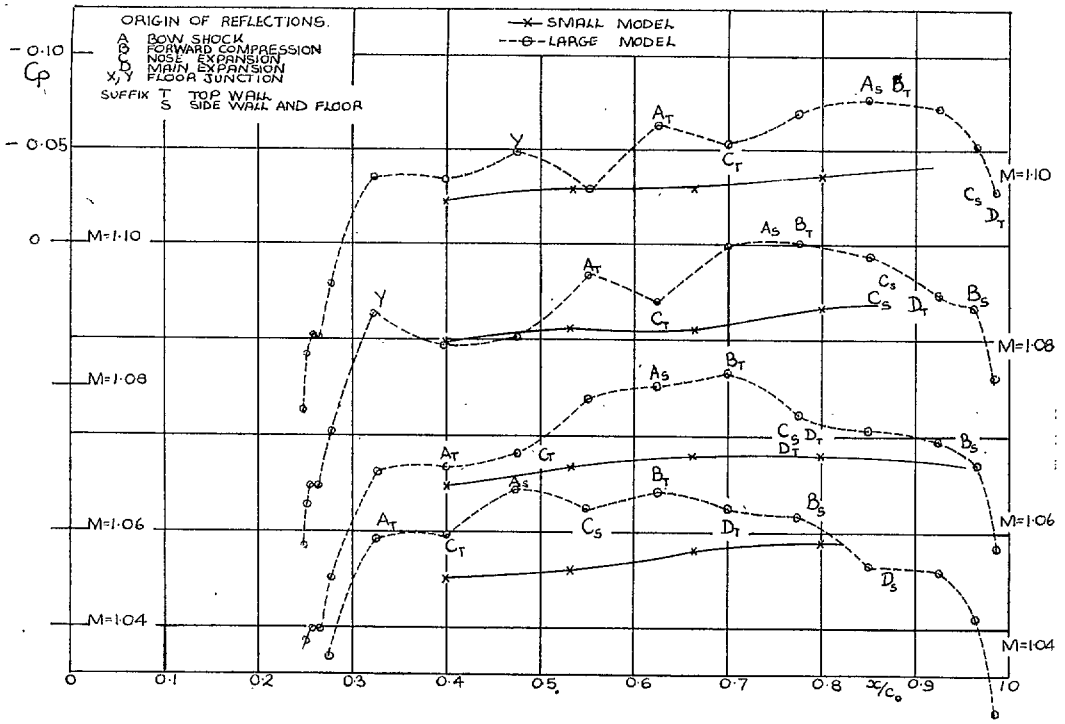

FIG. 12a. Chordwise C_p distributions. $\eta = 0{\cdot}25$.

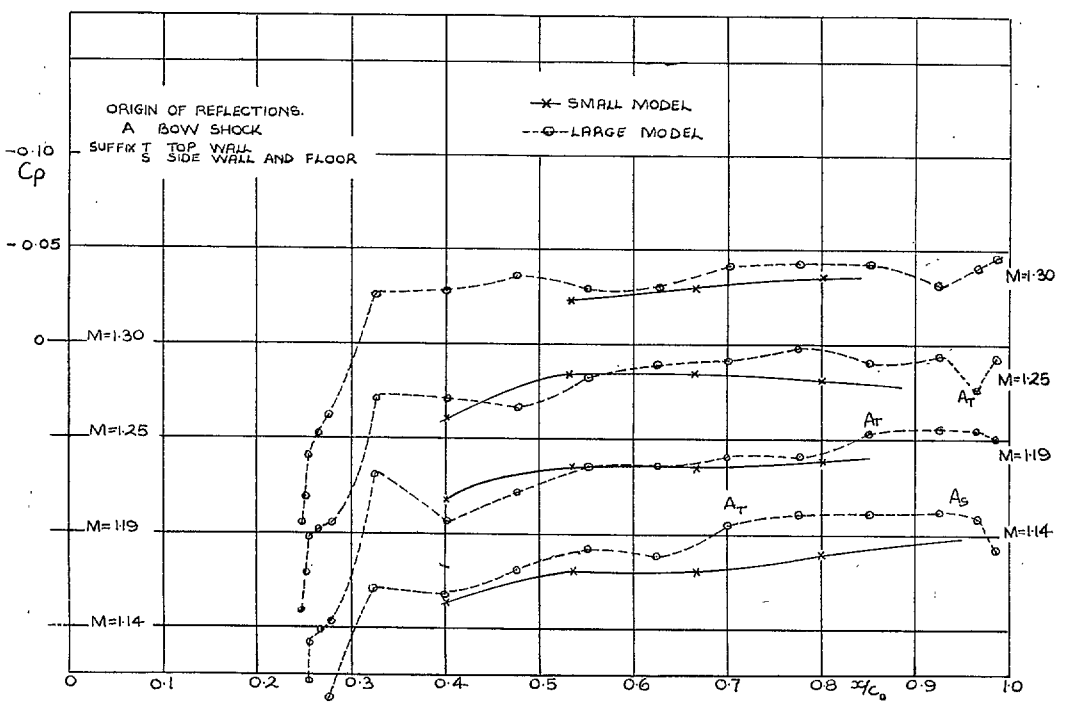

FIG. 12b. Chordwise C_p distributions. $\eta = 0{\cdot}25$.

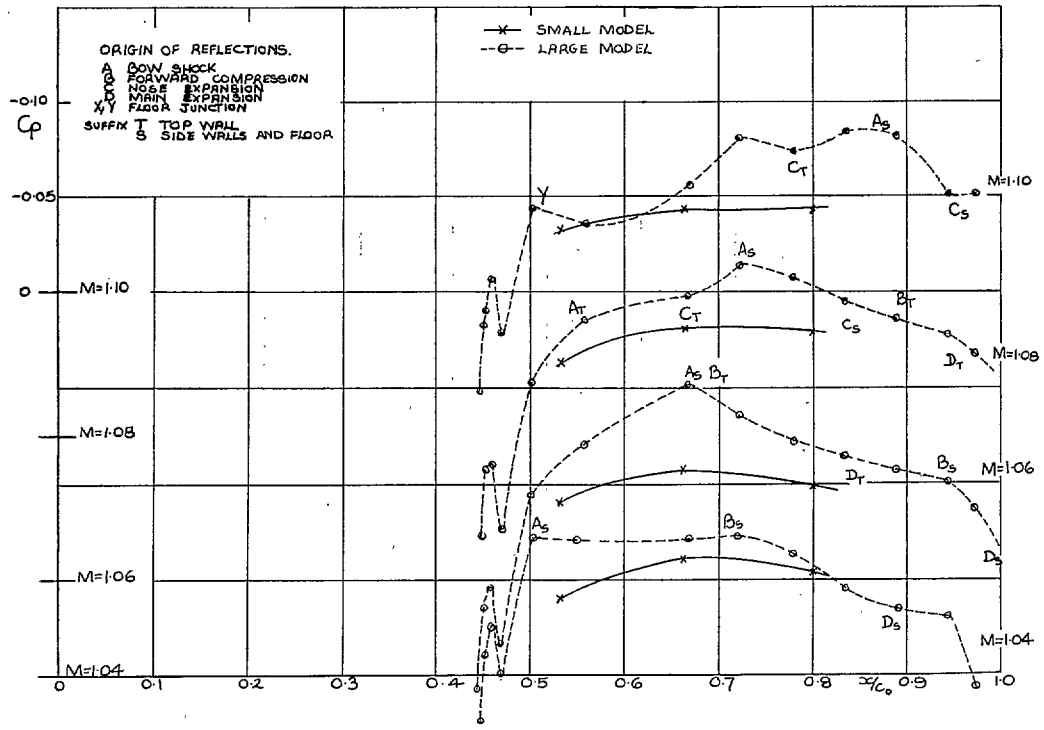

FIG. 13a. Chordwise C_p distributions. $\eta = 0{\cdot}45$.

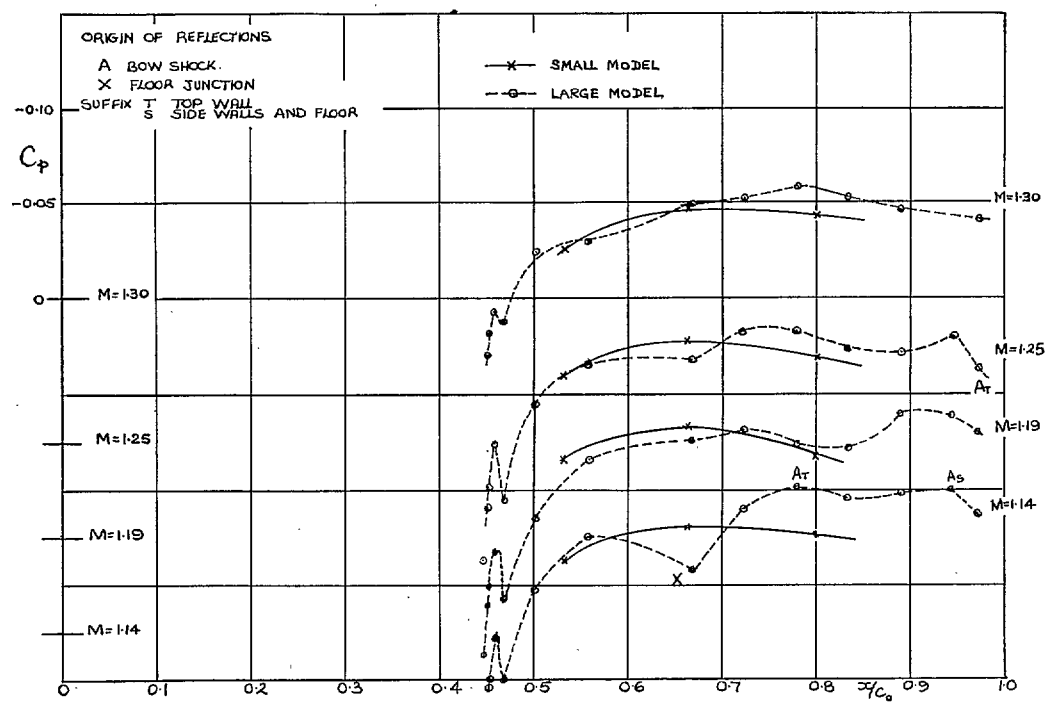

FIG. 13b. Chordwise C_p distributions. $\eta = 0{\cdot}45$.

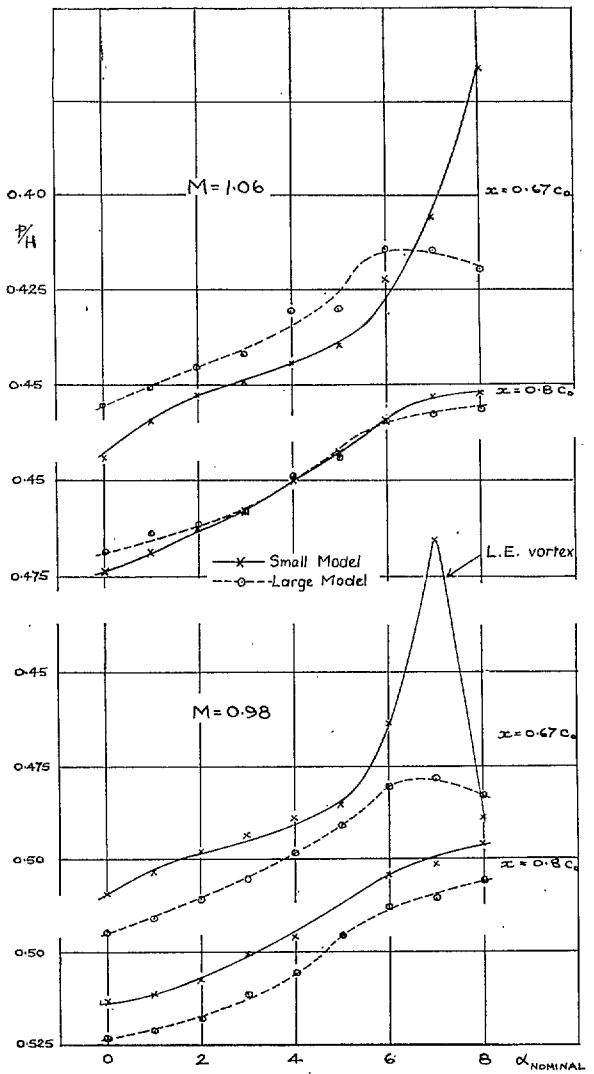

FIG. 14. Variation of p/H with incidence. $\eta = 0{\cdot}45$.

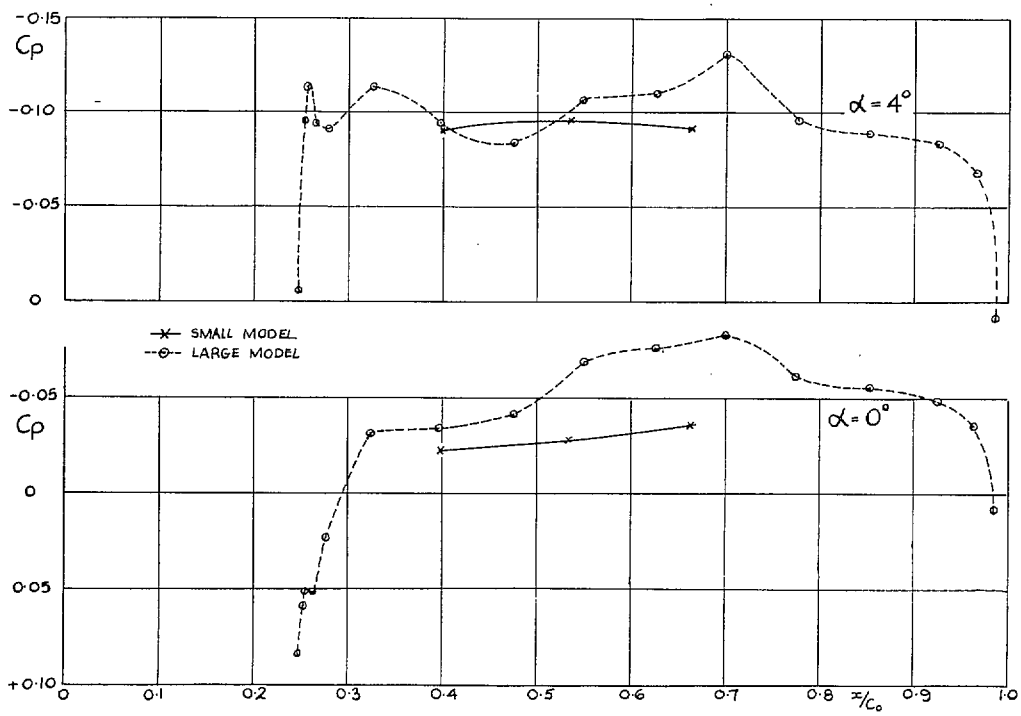

FIG. 15a. Effect of incidence on chordwise C_p distribution. $M = 1{\cdot}06$, $\eta = 0{\cdot}25$.

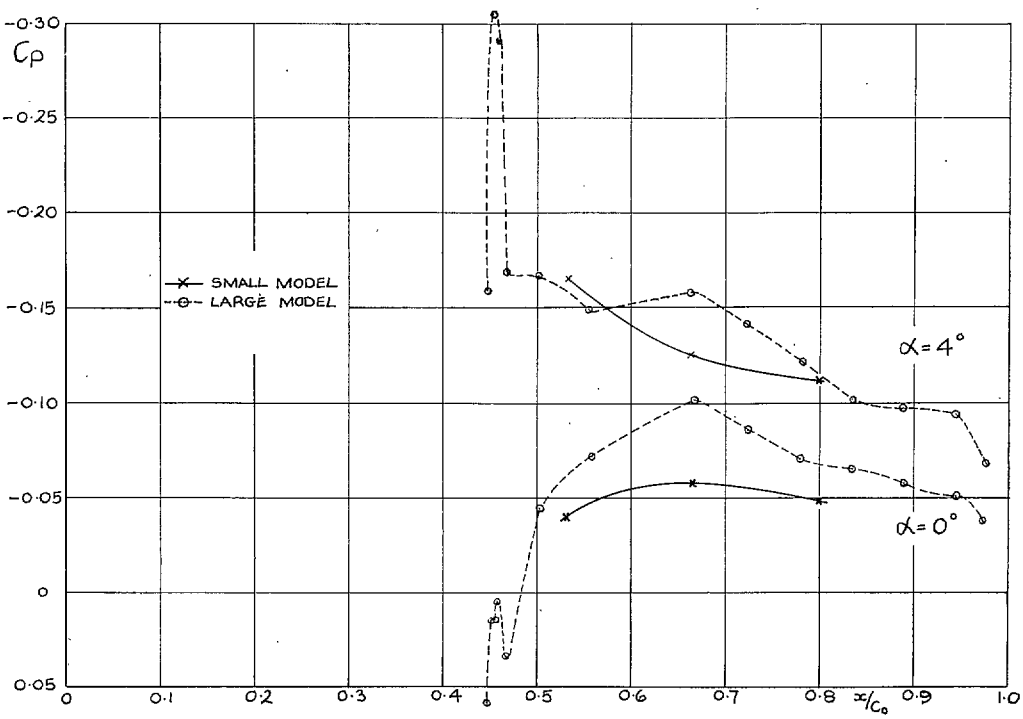

FIG. 15b. Effect of incidence on chordwise C_p distribution. $M = 1{\cdot}06$, $\eta = 0{\cdot}45$.

(85537) Wt. 64/1857 K. 5 9/62 Hw.

Publications of the Aeronautical Research Council

ANNUAL TECHNICAL REPORTS OF THE AERONAUTICAL RESEARCH COUNCIL (BOUND VOLUMES)

1942 Vol. I. Aero and Hydrodynamics, Aerofoils, Airscrews, Engines. 75*s.* (post 2*s.* 9*d.*)
Vol. II. Noise, Parachutes, Stability and Control, Structures, Vibration, Wind Tunnels. 47*s.* 6*d.* (post 2*s.* 3*d.*)

1943 Vol. I. Aerodynamics, Aerofoils, Airscrews. 80*s.* (post 2*s.* 6*d.*)
Vol. II. Engines, Flutter, Materials, Parachutes, Performance, Stability and Control, Structures. 90*s.* (post 2*s.* 9*d.*)

1944 Vol. I. Aero and Hydrodynamics, Aerofoils, Aircraft, Airscrews, Controls. 84*s.* (post 3*s.*)
Vol. II. Flutter and Vibration, Materials, Miscellaneous, Navigation, Parachutes, Performance, Plates and Panels, Stability, Structures, Test Equipment, Wind Tunnels. 84*s.* (post 3*s.*)

1945 Vol. I. Aero and Hydrodynamics, Aerofoils. 130*s.* (post 3*s.* 6*d.*)
Vol. II. Aircraft, Airscrews, Controls. 130*s.* (post 3*s.* 6*d.*)
Vol. III. Flutter and Vibration, Instruments, Miscellaneous, Parachutes, Plates and Panels, Propulsion. 130*s.* (post 3*s.* 3*d.*)
Vol. IV. Stability, Structures, Wind Tunnels, Wind Tunnel Technique. 130*s.* (post 3*s.* 3*d.*)

1946 Vol. I. Accidents, Aerodynamics, Aerofoils and Hydrofoils. 168*s.* (post 3*s.* 9*d.*)
Vol. II. Airscrews, Cabin Cooling, Chemical Hazards, Controls, Flames, Flutter, Helicopters, Instruments and Instrumentation, Interference, Jets, Miscellaneous, Parachutes. 168*s.* (post 3*s.* 3*d.*)
Vol. III. Performance, Propulsion, Seaplanes, Stability, Structures, Wind Tunnels. 168*s.* (post 3*s.* 6*d.*)

1947 Vol. I. Aerodynamics, Aerofoils, Aircraft. 168*s.* (post 3*s.* 9*d.*)
Vol. II. Airscrews and Rotors, Controls, Flutter, Materials, Miscellaneous, Parachutes, Propulsion, Seaplanes, Stability, Structures, Take-off and Landing. 168*s.* (post 3*s.* 9*d.*)

1948 Vol. I. Aerodynamics, Aerofoils, Aircraft, Airscrews, Controls, Flutter and Vibration, Helicopters, Instruments, Propulsion, Seaplane, Stability, Structures, Wind Tunnels. 130*s.* (post 3*s.* 3*d.*)
Vol. II. Aerodynamics, Aerofoils, Aircraft, Airscrews, Controls, Flutter and Vibration, Helicopters, Instruments, Propulsion, Seaplane, Stability, Structures, Wind Tunnels. 110*s.* (post 3*s.* 3*d.*)

Special Volumes

Vol. I. Aero and Hydrodynamics, Aerofoils, Controls, Flutter, Kites, Parachutes, Performance, Propulsion, Stability. 126*s.* (post 3*s.*)
Vol. II. Aero and Hydrodynamics, Aerofoils, Airscrews, Controls, Flutter, Materials, Miscellaneous, Parachutes, Propulsion, Stability, Structures. 147*s.* (post 3*s.*)
Vol. III. Aero and Hydrodynamics, Aerofoils, Airscrews, Controls, Flutter, Kites, Miscellaneous, Parachutes, Propulsion, Seaplanes, Stability, Structures, Test Equipment. 189*s.* (post 3*s.* 9*d.*)

Reviews of the Aeronautical Research Council

1939–48 3*s.* (post 6*d.*) 1949–54 5*s.* (post 5*d.*)

Index to all Reports and Memoranda published in the Annual Technical Reports

1909–1947 R. & M. 2600 (out of print)

Indexes to the Reports and Memoranda of the Aeronautical Research Council

Between Nos. 2351–2449	R. & M. No. 2450 2*s.* (post 3*d.*)
Between Nos. 2451–2549	R. & M. No. 2550 2*s.* 6*d.* (post 3*d.*)
Between Nos. 2551–2649	R. & M. No. 2650 2*s.* 6*d.* (post 3*d.*)
Between Nos. 2651–2749	R. & M. No. 2750 2*s.* 6*d.* (post 3*d.*)
Between Nos. 2751–2849	R. & M. No. 2850 2*s.* 6*d.* (post 3*d.*)
Between Nos. 2851–2949	R. & M. No. 2950 3*s.* (post 3*d.*)
Between Nos. 2951–3049	R. & M. No. 3050 3*s.* 6*d.* (post 3*d.*)
Between Nos. 3051–3149	R. & M. No. 3150 3*s.* 6*d.* (post 3*d.*)

HER MAJESTY'S STATIONERY OFFICE

from the addresses overleaf

Printed and published by
HER MAJESTY'S STATIONERY OFFICE

To be purchased from
York House, Kingsway, London W.C.2
423 Oxford Street, London W.1
13A Castle Street, Edinburgh 2
109 St. Mary Street, Cardiff
39 King Street, Manchester 2
50 Fairfax Street, Bristol 1
35 Smallbrook, Ringway, Birmingham 5
80 Chichester Street, Belfast 1
or through any bookseller

Printed in England

S.O. Code No. 23-3287